

A sharp-interface discontinuous Galerkin method for simulation of two-phase flow of real gases based on implicit shock tracking

Charles Naudet^{a,1}, Brian Taylor^{b,2}, Matthew J. Zahr^{a,3,*}

^aDepartment of Aerospace and Mechanical Engineering, University of Notre Dame, Notre Dame, IN 46556, United States

^bAir Force Research Laboratory, Eglin AFB, FL 32542

Abstract

We present a high-order, sharp-interface method for simulation of two-phase flow of real gases using implicit shock tracking. The method is based on a phase-field formulation of two-phase, compressible, inviscid flow with a trivial mixture model. Implicit shock tracking is a high-order, optimization-based discontinuous Galerkin method that automatically aligns mesh faces with non-smooth flow features to represent them perfectly with inter-element jumps. It is used to accurately approximate shocks and rarefactions without stabilization and converge the phase-field solution to a sharp interface one by aligning mesh faces with the material interface. Time-dependent problems are formulated as steady problems in a space-time domain where complex wave interactions (e.g., intersections and reflections) manifest as space-time triplet points. The space-time formulation avoids complex re-meshing and solution transfer that would be required to track moving waves with mesh faces using the method of lines. The approach is applied to several two-phase flow Riemann problems involving gases with ideal, stiffened gas, and Becker-Kistiakowsky-Wilson (BKW) equations of state, including a spherically symmetric underwater explosion problem. In all cases, the method aligns element faces with all shocks (including secondary shocks that form at time $t > 0$), rarefactions, and material interfaces, and accurately resolves the flow field on coarse space-time grids.

Keywords: Shock tracking, high-order methods, discontinuous Galerkin, two-phase flow, space-time methods, sharp-interface model

1. Introduction

Compressible, two-phase flows arise in the study of bubbles and interfaces [43, 58], mixing processes [72], bubbly flows [30, 37], granular solids [48, 49], and explosive mixtures [5, 16], to name a few. Such flows are challenging to simulate because treatment of the material interface plays a large role in the stability and accuracy of the method. We propose a novel simulation methodology for compressible, two-phase flow that circumvents several of the challenges faced by modern tools.

1.1. Review of two-phase flow simulation technology

Numerical methods to simulate two-phase flow either approximate the material interface as a smooth transition between materials (*diffuse interface*) or treat the interface as a true discontinuity in the material (*sharp interface*).

1.1.1. Diffuse-interface approaches

Shocks and material interfaces arise in compressible, two-phase flow simulations and lead to non-physical oscillations in the solution when greater-than-first-order discretization methods are used. In single-phase

*Corresponding author

¹Graduate Student, Department of Aerospace and Mechanical Engineering, University of Notre Dame

²Senior Research Engineer, Air Force Research Laboratory

³Assistant Professor, Department of Aerospace and Mechanical Engineering, University of Notre Dame

flow problems, these oscillations are suppressed using shock capturing methods such as limiting [69, 7], non-oscillatory reconstruction methods [20, 35], and artificial viscosity methods [46, 6], for example. For two-phase flows, conservative interface-capturing schemes diffuse the material interface, which leads to spurious oscillations from pressure calculations in the mixture region [5, 2]. Non-conservative [26, 27] and conservative [50, 61] interface-capturing methods based on the primitive form of the governing equations have been proposed to improve the accuracy of pressure computations near the interface. Other approaches to suppress non-physical oscillations near the material interface include specialized discretizations of the species mass fraction equation [1, 55], inclusion of an energy correction equation [23, 5], and introduction of a pressure non-equilibrium model that reduces to a single-velocity, single-pressure model [56, 28, 18]. Many of these approaches have been used in combination with high-order discretizations [29] such as discontinuous Galerkin (DG) [18, 13, 70] and weighted essentially non-oscillatory (WENO) reconstructions [24, 16] to increase accuracy per degree of freedom. However, these diffuse-interface methods will be, at best, first-order accurate near shocks or material interfaces because a smooth profile is being used to approximate a discontinuity. This is usually offset with significant adaptive mesh refinement near shocks and interfaces [5].

1.1.2. Sharp-interface approaches

In contrast to diffuse-interface methods, sharp-interface methods discretize the governing equations in each fluid domain separately, and interface conditions are used to evolve the material interface in time. Mesh-based Lagrangian methods [4, 25] deform the grid at each time step to align with the material interface, which ensures a sharp interface but leads to a distorted or tangled mesh for large interface deformations. Meshless Lagrangian methods [34, 65, 60] have been developed to address the mesh distortion problem; however, they suffer from their own shortcomings such as large computational cost, instabilities due to particle clustering, difficulty enforcing boundary conditions, and overall lower accuracy. Marker-and-cell (MAC) methods [19, 39] advect particles in a Lagrangian manner with the flow velocity to reconstruct a sharp interface. While accurate, this can be computationally expensive in three dimensions due to the large number of particles that must be tracked. Arbitrary Lagrangian-Eulerian [14, 12] and front-tracking [9] methods reduce the cost of MAC methods by only adding a set of connected marker particles to the material interface. These approaches tend to allow for larger interface deformations than pure Lagrangian approaches; however, they will still lead to distorted meshes for large deformations and cannot handle topological changes to the interface.

An alternative to Lagrangian or mixed Eulerian-Lagrangian approaches are pure Eulerian methods that use a fixed grid. These methods can be classified as either interface capturing (Section 1.1.1) or interface tracking. Interface-tracking methods combine the flow equations with a mathematical model to reconstruct the interface, e.g., such as volume of fluid (VOF) [53, 54, 42, 17, 71, 47] or level sets [45, 67, 66, 68]. The VOF method advects the volume fraction of each fluid using an interface advection equation and ensures mass conservation; however, geometric reconstruction of the interface is difficult and leads to accuracy degradation [42]. Level set methods [68, 66, 67, 57] implicitly define the interface through a signed distance function that is advected with the fluid velocity. These methods can reconstruct complex interface topologies and have proven to lead to highly accurate two-phase flow simulations, especially when coupled with high-order cut-cell methods [57, 33]. However, they violate mass conservation [66], require sufficiently smooth interfaces (to be represented by a level set function), incur additional cost from the level set advection equation, and are quite intricate.

Overall, sharp-interface methods avoid the non-physical numerical oscillations that arise at the material interface using diffuse-interface methods. However, these methods have their own shortcomings. They suffer from an accumulation of error in the location of the material interface as it evolves. They are strictly used to obtain a sharp material interface, whereas stabilization techniques must be used to resolve shock waves and other contact discontinuities, which degrades global solution accuracy to first-order. This can lead to further loss of accuracy if shock waves interact with the material interface.

1.2. Proposed approach: Sharp-interface method based on space-time implicit shock tracking

In this work, we propose a high-order DG discretization of two-phase flow with sharp interface treatment based on implicit shock tracking. Our approach uses the High-Order Implicit Shock Tracking (HOIST) method [73, 74, 22] to align the computational grid with all non-smooth flow features (shocks, material interfaces, head/tail of rarefactions) to represent them perfectly with inter-element jumps in the DG basis,

leaving the intra-element polynomial basis to represent smooth regions of the flow with high-order accuracy. Alignment of the mesh faces with non-smooth features is achieved without explicit shock detection or remeshing; rather, it is the solution of an optimization problem that minimizes the enriched DG residual (based on a test space with higher polynomial degree than the trial space) and therefore alignment is achieved implicitly. The optimization problem is initialized from a shock-agnostic grid.

Two variants of implicit shock tracking have been developed: (1) a method-of-lines approach [59] that solves an optimization problem at each time step to deform the grid as time evolves to ensure the same element faces track the non-smooth features as they evolve and (2) a space-time approach [10, 11, 40, 44] that recast the time-dependent problem in d' dimensions as a steady problem in $(d' + 1)$ dimensions and aligns element faces of the space-time mesh with the non-smooth features in space-time. The time domain in the latter approach is usually split into a number of slabs to avoid coupling the entire temporal domain. The method-of-lines approach is more efficient because it works directly with the unsteady conservation law without increasing the dimensionality of the problem; however, it will inevitably lead to mesh entanglement if the non-smooth features move substantially throughout the domain or intersect. On the other hand, these complex features manifest as curves and triple points in space-time, both of which are handled robustly by implicit shock tracking [10, 22, 40]. Thus, we build our method on space-time implicit shock tracking to robustly handle complex wave dynamics.

The space-time formulation of implicit shock tracking introduces a special complication for two-phase flow. Because the shock-aligned grid is computed as the solution of an optimization problem and initialized from a non-aligned grid, the material interface is not present until the end of the simulation making it difficult to assign an equation of state to each space-time location. We overcome this problem by introducing an additional equation governing the advection of the material phase, $\phi(x, t) \in [0, 1]$, where $\phi(x, t) = 1$ means material 1 occupies the space-time point (x, t) , $\phi(x, t) = 0$ means material 2 occupies the point, and $0 < \phi(x, t) < 1$ represent a non-physical mixture of the phases. Because we are using implicit shock tracking to represent the interface as a perfect discontinuity, we expect $\phi(x, t) \in \{0, 1\}$ at convergence. Thus, non-trivial mixtures are only used to help discover the true interface location. As a result, the mixture equation of state must only be thermodynamically consistent with the individual materials in the limit as $\phi \rightarrow 0$ and $\phi \rightarrow 1$. Other approaches that employ a phase variable have stringent requirements on the mixture equation of state for $0 < \phi < 1$ [64].

To demonstrate the proposed approach, we consider a one-dimensional Riemann problem of the Euler equations (27) involving two ideal gases with initial condition

$$\rho(x, 0) = \begin{cases} 1 & x < 0.4 \\ \alpha & x \geq 0.5 \\ 0.125 & \text{else} \end{cases}, \quad v(x, 0) = \begin{cases} 0 & x < 0.4 \\ \beta & x \geq 0.5 \\ 0 & \text{else} \end{cases}, \quad P(x, 0) = \begin{cases} 0.1 & x < 0.4 \\ \omega & x \geq 0.5 \\ 0.1 & \text{else} \end{cases}, \quad \gamma(x, 0) = \begin{cases} 5/3 & x < 0.4 \\ 5/3 & x \geq 0.5 \\ 7/5 & \text{else} \end{cases} \quad (1)$$

where $\rho(x, t) \in \mathbb{R}_{>0}$ is the density of the fluid at $x \in \Omega_x := (0, 1)$ and $t \in \mathcal{T} := (0, 0.2]$, $v(x, t) \in \mathbb{R}$ is the velocity of the fluid at $(x, t) \in \Omega_x \times \mathcal{T}$, $P(x, t) \in \mathbb{R}_{\geq 0}$ is the pressure of the fluid at $(x, t) \in \Omega_x \times \mathcal{T}$, and $\gamma(x, t) \in \mathbb{R}_{\geq 0}$ is the ratio of specific heats at $(x, t) \in \Omega_x \times \mathcal{T}$, and $\alpha = 0.4263194281784951$, $\beta = -0.92745262004894879$, $\omega = 0.30313017805064679$. This problem features a stationary material interface at $x = 0.4$ and a left-moving shock and material interface at $x = 0.5$. Once the shock impinges on the stationary interface, the material interface begins to move and both a reflected and pass-through shock are created. The proposed approach is initialized from a first-order solution on a shock-agnostic mesh, which includes material mixtures because the mesh is not aligned with the interface yet. However, at convergence, mesh faces are aligned with the interface, which allows the contact discontinuity to be represented perfectly and a solution completely devoid of mixtures is obtained (Figure 1-2). The shock-contact interaction and subsequent shock reflection in the space-time solution would require re-meshing and solution transfer in the method-of-lines setting. However, these simply manifest as triple points in space-time, which are handled robustly by implicit shock tracking.

1.3. Contributions

The contributions of this work are three-fold. First and foremost, the proposed high-order sharp-interface methodology for real gas two-phase flow simulations based on implicit shock tracking is novel. The method overcomes many of the traditional challenges of sharp-interface approaches to two-phase flow at the cost of increased complexity and computational expense from the space-time formulation. A similar approach

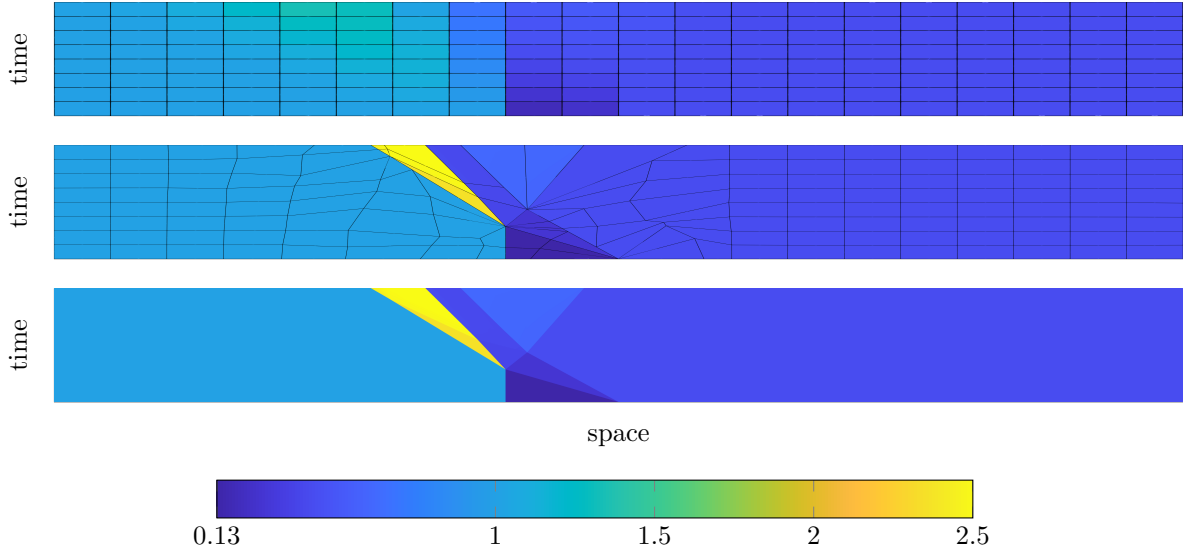


Figure 1: Shock-agnostic space-time mesh and first-order solution (density) used to initialize HOIST solver (*top*), and converged HOIST solution (density) with (*middle*) and without (*bottom*) mesh edges.

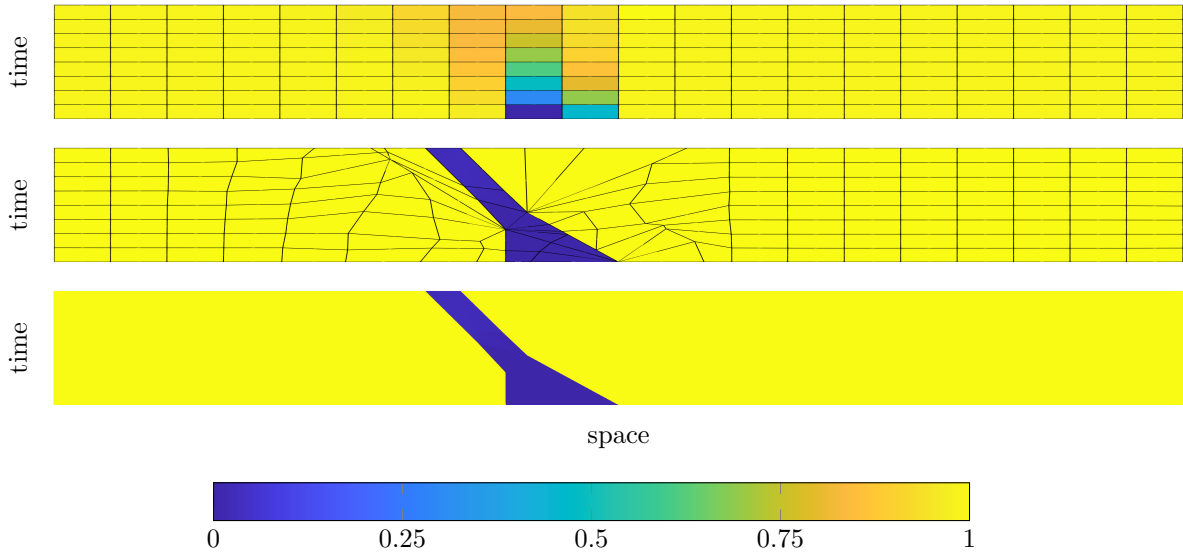


Figure 2: Shock-agnostic space-time mesh and first-order solution (phase) used to initialize HOIST solver (*top*), and converged HOIST solution (phase) with (*middle*) and without (*bottom*) mesh edges.

[10, 11, 44] uses the Moving Discontinuous Galerkin Method with Interface Condition Enforcement (MDG-ICE) version of implicit shock fitting instead of HOIST for ideal gases. This work also presents the flux Jacobian and its complete eigenvalue decomposition for both a single- and two-phase real gas in multiple spatial dimensions. These eigenvalue decompositions are used to construct upwinded numerical flux functions (e.g., Roe’s flux [51]); however, they are usually only presented in one dimension [55].

1.4. Outline

The remainder of this paper is organized as follows. Section 2 systematically builds up a space-time formulation of a time-dependent conservation law from a traditional formulation that separates the temporal and spatial independent variables and transforms the space-time conservation law to a reference domain such that domain deformations appear explicitly in the conservation law. This section specializes this general formulation to the single- and two-phase, compressible Euler equations, including a complete description the flux Jacobians and their eigenvalue decompositions (commonly use to build numerical flux functions). The section closes with an overview of the three equations of state considered in this work (ideal gas, stiffened gas, and Becker-Kistiakowsky-Wilson model). Section 3 details a high-order DG discretization of the transformed space-time conservation law. Section 4 uses this discretization to formulate the implicit shock tracking method and review relevant details in the space-time setting from [40]. Section 5 applies the proposed methods to a sequence of increasingly difficult problems beginning with a simple single-phase validation case and closes with a spherically symmetric underwater blast problem. Finally, Section 6 offers conclusions.

2. Governing equations

In this section we introduce the governing equations considered in this manuscript, namely, inviscid, compressible single- and two-phase flow involving real gases. We begin with a general form of a time-dependent, inviscid conservation law (Section 2.1), its formulation as a space-time conservation law (Section 2.2), and a reformulation of the space-time conservation law on a fixed reference domain (Section 2.3) because the proposed shock tracking method will deform the space-time domain to align element faces with discontinuities. Next, we introduce the Euler equations of gasdynamics for single-phase (Section 2.4) and two-phase (Section 2.5) of real gases with a generic equation of state. The inviscid projected Jacobian and its analytical eigenvalue decomposition are provided as these play a key role in the construction of numerical fluxes schemes [15]. We use a phase variable to track the two phases with the mixture model described in Section 2.6. We close this section with the specific real gases considered in the numerical experiments (Section 2.7) to demonstrate the versatility of the framework in Sections 2.4-2.5 for any equation of state.

2.1. Time-dependent system of conservation laws

Consider a general system of m hyperbolic partial differential equations posed in the spatial domain $\Omega_x \subset \mathbb{R}^{d'}$ over the time interval $\mathcal{T} := (t_0, t_1) \subset \mathbb{R}_{\geq 0}$

$$\frac{\partial U_x}{\partial t} + \nabla_x \cdot \mathcal{F}_x(U_x) = \mathcal{S}_x(U_x), \quad (2)$$

where $t \in \mathcal{T}$ is the temporal coordinate, $x = (x_1, \dots, x_{d'}) \in \Omega_x$ is the spatial coordinate, $U_x(\cdot, t) : \Omega_x \rightarrow \mathbb{R}^m$ is the conservative state implicitly defined as the solution to (2), $\mathcal{F}_x : \mathbb{R}^m \rightarrow \mathbb{R}^{m \times d'}$ with $\mathcal{F}_x : W_x \mapsto \mathcal{F}_x(W_x)$ is the physical flux function, $\mathcal{S}_x : \mathbb{R}^m \rightarrow \mathbb{R}^m$ is the physical source term, $(\nabla_x \cdot)$ is the divergence operator on the domain Ω_x defined as $(\nabla_x \cdot \psi)_i := \partial_{x_j} \psi_{ij}$ (summation implied on repeated index), and $\partial\Omega_x$ is the boundary of the spatial domain (with appropriate boundary conditions prescribed). In general, the solution $U(x, t)$ may contain discontinuities, in which case, the conservation law (2) holds away from the discontinuities and the Rankine-Hugoniot conditions hold at discontinuities.

The Jacobian of the projected inviscid flux is

$$B_x : \mathbb{R}^m \times \mathbb{S}_{d'} \rightarrow \mathbb{R}^{m \times m}, \quad B_x : (W_x, \eta_x) \mapsto \frac{\partial[\mathcal{F}_x(W_x)\eta_x]}{\partial W_x}, \quad (3)$$

where $\mathbb{S}_{d'} := \{\eta \in \mathbb{R}^{d'} \mid \|\eta\| = 1\}$. The eigenvalue decomposition of the Jacobian is

$$B_x(W_x, \eta_x) = V_x(W_x, \eta_x) \Lambda_x(W_x, \eta_x) V_x(W_x, \eta_x)^{-1}, \quad (4)$$

where $\Lambda_x : \mathbb{R}^m \times \mathbb{S}_{d'} \rightarrow \mathbb{R}^{m \times m}$ is a diagonal matrix containing the real eigenvalues of B_x and the columns of $V_x : \mathbb{R}^m \times \mathbb{S}_{d'} \rightarrow \mathbb{R}^{m \times m}$ contain the corresponding right eigenvectors.

2.2. Space-time formulation

The conservation law in (2) describes a general time-dependent system of conservation laws in a d' -dimensional spatial domain. Because the proposed method tracks discontinuities over space-time slabs, we reformulate (2) as a steady conservation law in a space-time domain [36, 63, 32]. To this end, we define the space-time domain as $\Omega := \Omega_x \times \mathcal{T} \subset \mathbb{R}^d$ ($d = d' + 1$) with boundary $\partial\Omega$, and let $z = (x, t) \in \Omega$ denote the space-time coordinate. Because the space-time domain is a Cartesian product of the spatial domain with a time interval, we will refer to it as a *space-time slab*. The temporal domain \mathcal{T} may be the entire time window of interest, or a portion of it. The boundary of a space-time slab $\partial\Omega$ consists of three pieces: 1) the spatial boundary, $\partial\Omega_x \times \mathcal{T}$, 2) the bottom of the slab, $\Omega_x \times \{t_0\}$, and 3) the top of the slab, $\Omega_x \times \{t_1\}$. Without loss of generality, we formulate the space-time conservation law, as well as its transformation (Section 2.2) and discretization (Section 3) over a single arbitrary slab corresponding to the time interval \mathcal{T} ; in practice, we use a sequence of space-time slabs to cover the temporal domain of interest.

The conservation law in (2) can be written as a steady conservation law over the space-time slab as

$$\nabla \cdot \mathcal{F}(U) = \mathcal{S}(U), \quad (5)$$

where $U : \Omega \rightarrow \mathbb{R}^m$ is the space-time conservative vector implicitly defined as the solution of (5) and related to the solution of the spatial conservation law as $U : z \mapsto U_x(x, t)$, $\mathcal{F} : \mathbb{R}^m \rightarrow \mathbb{R}^{m \times d}$ and $\mathcal{S} : \mathbb{R}^m \rightarrow \mathbb{R}^{m \times d}$ are the space-time flux function and source term, respectively, and related to the spatial conservation law terms as

$$\mathcal{F} : W \mapsto [\mathcal{F}_x(W) \quad W], \quad \mathcal{S} : W \mapsto \mathcal{S}_x(W), \quad (6)$$

and $(\nabla \cdot)$ is the space-time divergence operator defined as $\nabla \cdot [\psi \quad \phi] = \nabla_x \cdot \psi + \partial_t \phi$.

The Jacobian of the space-time projected inviscid flux $B : \mathbb{R}^m \times \mathbb{S}_d \rightarrow \mathbb{R}^{m \times m}$ is

$$B : (W, \eta) \mapsto \frac{\partial[\mathcal{F}(W)\eta]}{\partial W}. \quad (7)$$

Any $\eta \in \mathbb{S}_d$ can be written as $\eta = (n_x, n_t)$ where $n_x \in \mathbb{R}^d$ and $n_t \in \mathbb{R}$, and n_x can be expanded $n_x = \eta_x \|n_x\|$ with $\eta_x \in \mathbb{S}_{d'}$ (η_x is uniquely defined as $n_x / \|n_x\|$ in the case where $n_x \neq 0$, otherwise it is arbitrary). From this expansion and the form of the inviscid flux in (6), the space-time Jacobian can be related to the original Jacobian

$$B(W, \eta) = B_x(W, \eta_x) \|n_x\| + n_t I_m. \quad (8)$$

The eigenvalue decomposition of the projected Jacobian is denoted

$$B(W, \eta) = V(W, \eta) \Lambda(W, \eta) V(W, \eta)^{-1}, \quad (9)$$

where $\Lambda : \mathbb{R}^m \times \mathbb{S}_d$ is a diagonal matrix containing the real eigenvalues of B and the columns of $V : \mathbb{R}^m \times \mathbb{S}_d \rightarrow \mathbb{R}^{m \times m}$ contain the corresponding right eigenvectors. Owing to the relationship between the projected Jacobians of the spatial and space-time inviscid fluxes (8), their eigenvalue decompositions are related as

$$\Lambda(W, \eta) = \Lambda_x(W, \eta_x) \|n_x\| + n_t I_m, \quad V(W, \eta) = V_x(W, \eta_x) \quad (10)$$

2.3. Transformed space-time conservation law on a fixed reference domain

Because the proposed numerical method is based on deforming the space-time domain to track discontinuities with the computational grid, it is convenient to recast the space-time conservation law such that domain deformations appear explicitly. To this end, we define $\bar{\Omega} \subset \mathbb{R}^d$ as a fixed space-time reference domain, which we require to take the form of a space-time slab, i.e., $\bar{\Omega} := \Omega_x \times \mathcal{T}$. Let \mathbb{G} be the collection of diffeomorphisms from the reference domain to the physical domain, i.e., for any $\mathcal{G} \in \mathbb{G}$, $\mathcal{G} : \bar{\Omega} \rightarrow \Omega$ with $\mathcal{G} : \bar{z} \mapsto \mathcal{G}(\bar{z})$, that

preserve the space-time slab structure of the physical domain. The space-time conservation law in (5) can be reformulated as a conservation law over the reference domain as [73, 40]

$$\bar{\nabla} \cdot \bar{\mathcal{F}}(\bar{U}; G) = \bar{S}(\bar{U}; g), \quad (11)$$

where $\bar{U} : \bar{\Omega} \rightarrow \mathbb{R}^m$ is the solution of the transformed conservation law, $\bar{\mathcal{F}} : \mathbb{R}^m \times \mathbb{R}^{d \times d} \rightarrow \mathbb{R}^{m \times d}$ and $\bar{S} : \mathbb{R}^m \times \mathbb{R} \rightarrow \mathbb{R}^m$ are the transformed flux function and source term, respectively, $\bar{\nabla} \cdot$ is the divergence operator in the reference domain $\bar{\Omega}$ defined as $(\bar{\nabla} \cdot \psi)_i = \partial_{\bar{z}_j} \psi_{ij}$, and the deformation gradient $G : \bar{\Omega} \rightarrow \mathbb{R}^{d \times d}$ and mapping Jacobian $g : \bar{\Omega} \rightarrow \mathbb{R}$ are

$$G : \bar{z} \mapsto \partial_{\bar{z}} \mathcal{G}(\bar{z}), \quad g : \bar{z} \mapsto \det G(\bar{z}). \quad (12)$$

The reference domain quantities are defined in terms of the corresponding physical domain quantities as [73]

$$\bar{U}(\bar{z}) = U(\mathcal{G}(\bar{z})), \quad \bar{\mathcal{F}} : (\bar{W}; \Theta) \mapsto (\det \Theta) \mathcal{F}(\bar{W}) \Theta^{-T}, \quad \bar{S} : (\bar{W}; q) \mapsto q S(\bar{W}). \quad (13)$$

2.4. Inviscid, compressible single-phase flow of real gas

Consider flow of an inviscid, compressible fluid through a domain $\Omega_x \subset \mathbb{R}^{d'}$, where $d' \geq 1$ is the spatial dimension, governed by the Euler equations (2) with

$$U_x = \begin{bmatrix} \rho \\ \rho v \\ \rho E \end{bmatrix}, \quad \mathcal{F}_x(U_x) = \begin{bmatrix} \rho v^T \\ \rho v v^T + P(\rho, e) I_{d'} \\ [\rho E + P(\rho, e)] v^T \end{bmatrix}, \quad \mathcal{S}_x(U_x) = 0, \quad (14)$$

where $\rho : \Omega_x \times \mathcal{T} \rightarrow \mathbb{R}_{\geq 0}$ is the density of the fluid, $v : \Omega_x \times \mathcal{T} \rightarrow \mathbb{R}^{d'}$ is the velocity of the fluid, $E : \Omega_x \times \mathcal{T} \rightarrow \mathbb{R}$ is the total energy of the fluid, and $e : \Omega_x \times \mathcal{T} \rightarrow \mathbb{R}_{\geq 0}$ is the specific internal energy of the fluid. The *equation of state* defines the pressure of the fluid, $P : \mathbb{R}_{\geq 0} \times \mathbb{R}_{\geq 0} \rightarrow \mathbb{R}_{\geq 0}$, as a function of its density and specific internal energy, i.e., $P : (\rho, e) \mapsto P(\rho, e)$. The partial derivatives of this function play a central role in the flux Jacobian and its eigenvalue decomposition so we introduce the following short-hand notation: $P_\rho : \mathbb{R}_{\geq 0} \times \mathbb{R}_{\geq 0} \rightarrow \mathbb{R}$ and $P_e : \mathbb{R}_{\geq 0} \times \mathbb{R}_{\geq 0} \rightarrow \mathbb{R}$, defined as

$$P_\rho : (\rho, e) \mapsto \left. \frac{\partial P}{\partial \rho}(\rho, e) \right|_e, \quad P_e : (\rho, e) \mapsto \left. \frac{\partial P}{\partial e}(\rho, e) \right|_\rho \quad (15)$$

The internal energy relates to the conservative variables as

$$e(\rho, \rho v, \rho E) = \frac{\rho E}{\rho} - \frac{\rho v \cdot \rho v}{2\rho^2} \quad (16)$$

and enthalpy of the fluid is defined as $H = (\rho E + P)/\rho$. For convenience, we introduce a new function, \bar{P} , that represents the pressure *as a function of the conservative variables*

$$\bar{P} : \mathbb{R}_{\geq 0} \times \mathbb{R}^{d'} \times \mathbb{R} \rightarrow \mathbb{R}_{\geq 0}, \quad \bar{P} : (\rho, \rho v, \rho E) \mapsto P(\rho, e(\rho, \rho v, \rho E)). \quad (17)$$

This new definition will allow us to easily distinguish between derivatives of pressure under constant internal energy versus the derivatives of pressure under constant momentum or total energy without cumbersome notation. We use the chain rule to obtain the following expressions for the derivatives of pressure with the conservative variables held constant

$$\begin{aligned} \left. \frac{\partial \bar{P}}{\partial \rho}(\rho, \rho v, \rho E) \right|_{\rho v, \rho E} &= \left. \frac{\partial P}{\partial \rho}(\rho, e) \right|_e + \left. \frac{\partial P}{\partial e}(\rho, e) \right|_\rho \left. \frac{\partial e}{\partial \rho}(\rho, \rho v, \rho E) \right|_{\rho v, \rho E} = P_\rho(\rho, e) - \frac{P_e(\rho, e)}{\rho} (E - \|v\|^2) \\ \left. \frac{\partial \bar{P}}{\partial \rho v}(\rho, \rho v, \rho E) \right|_{\rho, \rho E} &= \left. \frac{\partial P}{\partial e}(\rho, e) \right|_\rho \left. \frac{\partial e}{\partial \rho v}(\rho, \rho v, \rho E) \right|_{\rho, \rho E} = -\frac{P_e(\rho, e)}{\rho} v \\ \left. \frac{\partial \bar{P}}{\partial \rho E}(\rho, \rho v, \rho E) \right|_{\rho, \rho v} &= \left. \frac{\partial P}{\partial e}(\rho, e) \right|_\rho \left. \frac{\partial e}{\partial \rho E}(\rho, \rho v, \rho E) \right|_{\rho, \rho v} = \frac{P_e(\rho, e)}{\rho}. \end{aligned} \quad (18)$$

For brevity, we introduce the following short-hand notation: $\bar{P}_\rho : \mathbb{R}_{\geq 0} \times \mathbb{R}^{d'} \times \mathbb{R} \rightarrow \mathbb{R}$, $\bar{P}_{\rho v} : \mathbb{R}_{\geq 0} \times \mathbb{R}^{d'} \times \mathbb{R} \rightarrow \mathbb{R}^{d'}$, $\bar{P}_{\rho E} : \mathbb{R}_{\geq 0} \times \mathbb{R}^{d'} \times \mathbb{R} \rightarrow \mathbb{R}$, defined as

$$\begin{aligned}\bar{P}_\rho : (\rho, \rho v, \rho E) &\mapsto \left. \frac{\partial \bar{P}}{\partial \rho}(\rho, \rho v, \rho E) \right|_{\rho v, \rho E}, \\ \bar{P}_{\rho v} : (\rho, \rho v, \rho E) &\mapsto \left. \frac{\partial \bar{P}}{\partial \rho v}(\rho, \rho v, \rho E) \right|_{\rho, \rho E}, \\ \bar{P}_{\rho E} : (\rho, \rho v, \rho E) &\mapsto \left. \frac{\partial \bar{P}}{\partial \rho E}(\rho, \rho v, \rho E) \right|_{\rho, \rho v}.\end{aligned}\tag{19}$$

From these definitions, the spatial projected inviscid Jacobian for the Euler equations with a general equation of state is

$$B_x : (U_x, \eta_x) \mapsto \begin{bmatrix} 0 & \eta_x^T & 0 \\ -v_n v + \bar{P}_\rho \eta_x & v_n I_{d'} + v \eta_x^T + \eta_x \bar{P}_{\rho v}^T & \bar{P}_{\rho E} \eta_x \\ (\bar{P}_\rho - H) v_n & H \eta_x^T + v_n \bar{P}_{\rho v}^T & (1 + \bar{P}_{\rho E}) v_n \end{bmatrix},\tag{20}$$

which, using (18), simplifies to

$$B_x : (U_x, \eta_x) \mapsto \begin{bmatrix} 0 & \eta_x^T & 0 \\ -v_n v + \bar{P}_\rho \eta_x & v_n I_{d'} + v \eta_x^T - \frac{P_e}{\rho} \eta_x v^T & \frac{P_e}{\rho} \eta_x \\ (\bar{P}_\rho - H) v_n & H \eta_x^T - v_n \frac{P_e}{\rho} v^T & \left(1 + \frac{P_e}{\rho}\right) v_n \end{bmatrix},\tag{21}$$

where $\eta_x \in \mathbb{R}^{d'}$ is the unit normal, $v_n := v \cdot \eta_x$, and $I_{d'}$ is the $d' \times d'$ identity matrix. The matrix of right eigenvectors is given by

$$V_x : (U_x, \eta_x) \mapsto \begin{bmatrix} 1 & \eta_x^T & 1 \\ v - c \eta_x & (v - \eta_x) \eta_x^T + I_{d'} & v + c \eta_x \\ H - v_n c & v^T + (\theta - v_n) \eta_x^T & H + v_n c \end{bmatrix},\tag{22}$$

where θ is defined as

$$\theta = \|v\|^2 - \bar{P}_\rho \frac{\rho}{P_e}.\tag{23}$$

The sound speed, c , is defined as

$$c^2 = \bar{P}_\rho + (H - \|v\|^2) \frac{P_e}{\rho};\tag{24}$$

see [Appendix B.1](#) for derivation. The diagonal matrix of eigenvalues corresponding to these right eigenvectors is

$$\Lambda_x : (U_x, \eta_x) \mapsto \begin{bmatrix} v_n - c & 0 & 0 \\ 0 & v_n I_{d'} & 0 \\ 0 & 0 & v_n + c \end{bmatrix}\tag{25}$$

Finally, the matrix of left eigenvectors is given by

$$V_x^{-1} : (U_x, \eta_x) \mapsto \frac{1}{2c^2 \rho} \begin{bmatrix} \rho \bar{P}_\rho + c \rho v_n & -c \rho \eta_x^T - P_e v^T & P_e \\ 2c^2 \rho (\eta_x v_n - v) + 2 \eta_x \omega & 2c^2 \rho (I_{d'} - \eta_x \eta_x^T) + 2 P_e \eta_x v^T & -2 \eta_x P_e \\ \rho \bar{P}_\rho - c \rho v_n & c \rho \eta_x^T - P_e v^T & P_e \end{bmatrix},\tag{26}$$

where $\omega = P_e (H - \|v\|^2)$.

2.5. Inviscid, compressible two-phase flow of real gases

Next, consider flow of two inviscid, compressible fluids through a domain $\Omega_x \subset \mathbb{R}^{d'}$, where $d' \geq 1$ is the spatial dimension, governed by the Euler equations using a phase variable with interface advection equation [64] (2) with

$$U_x = \begin{bmatrix} \rho \\ \rho v \\ \rho E \\ \rho \phi \end{bmatrix}, \quad \mathcal{F}_x(U_x) = \begin{bmatrix} \rho v^T \\ \rho v v^T + P(\rho, e, \rho \phi) I_{d'} \\ [\rho E + P(\rho, e, \rho \phi)] v^T \\ \rho \phi v^T \end{bmatrix}, \quad \mathcal{S}_x(U_x) = 0,\tag{27}$$

where ρ , v , and E are defined in Section 2.4, and $\phi : \Omega_x \times \mathcal{T} \rightarrow [0, 1]$ tracks the phase of the fluid, i.e., if $\phi(x, t) = 1$ then the fluid 1 occupies $x \in \Omega_x$ at time t , if $\phi(x, t) = 0$ then fluid 2 occupies $x \in \Omega_x$ at time t , otherwise some mixture of the two fluids (Section 2.6) occupies the space-time location. In the two-phase setting, the equation of state defines the pressure of the fluid, $P : \mathbb{R}_{\geq 0} \times \mathbb{R}_{\geq 0} \times \mathbb{R}_{\geq 0} \rightarrow \mathbb{R}_{\geq 0}$, as a function of its density, specific internal energy, and phase, i.e., $P : (\rho, e, \rho\phi) \mapsto P(\rho, e, \rho\phi)$. We use the following short-hand notation for the partial derivatives of this function: $P_\rho : \mathbb{R}_{\geq 0} \times \mathbb{R}_{\geq 0} \times \mathbb{R}_{\geq 0} \rightarrow \mathbb{R}$ and $P_e : \mathbb{R}_{\geq 0} \times \mathbb{R}_{\geq 0} \times \mathbb{R}_{\geq 0} \rightarrow \mathbb{R}$, defined as

$$P_\rho : (\rho, e, \rho\phi) \mapsto \left. \frac{\partial P}{\partial \rho}(\rho, e, \rho\phi) \right|_{e, \rho\phi}, \quad P_e : (\rho, e, \rho\phi) \mapsto \left. \frac{\partial P}{\partial e}(\rho, e, \rho\phi) \right|_{\rho, \rho\phi}. \quad (28)$$

Following Section 2.4 we introduce a new function, \bar{P} , that represents the pressure as a function of the conservative variables

$$\bar{P} : \mathbb{R}_{\geq 0} \times \mathbb{R}^{d'} \times \mathbb{R} \times \mathbb{R}_{\geq 0} \rightarrow \mathbb{R}_{\geq 0}, \quad \bar{P} : (\rho, \rho v, \rho E, \rho\phi) \mapsto P(\rho, e(\rho, \rho v, \rho E), \rho\phi). \quad (29)$$

We use the chain rule to obtain the following expressions for the derivatives of pressure with the conservative variables held constant

$$\begin{aligned} \left. \frac{\partial \bar{P}}{\partial \rho}(\rho, \rho v, \rho E, \rho\phi) \right|_{\rho v, \rho E, \rho\phi} &= \left. \frac{\partial P}{\partial \rho}(\rho, e, \rho\phi) \right|_{e, \rho\phi} + \left. \frac{\partial P}{\partial e}(\rho, e, \rho\phi) \right|_{\rho, \rho\phi} \left. \frac{\partial e}{\partial \rho}(\rho, \rho v, \rho E) \right|_{\rho v, \rho E} \\ \left. \frac{\partial \bar{P}}{\partial \rho v}(\rho, \rho v, \rho E, \rho\phi) \right|_{\rho, \rho E, \rho\phi} &= \left. \frac{\partial P}{\partial e}(\rho, e, \rho\phi) \right|_{\rho, \rho\phi} \left. \frac{\partial e}{\partial \rho v}(\rho, \rho v, \rho E, \rho\phi) \right|_{\rho, \rho E, \rho\phi} = -\frac{P_e(\rho, e, \rho\phi)}{\rho} v \\ \left. \frac{\partial \bar{P}}{\partial \rho E}(\rho, \rho v, \rho E, \rho\phi) \right|_{\rho, \rho v, \rho\phi} &= \left. \frac{\partial P}{\partial e}(\rho, e, \rho\phi) \right|_{\rho, \rho\phi} \left. \frac{\partial e}{\partial \rho E}(\rho, \rho v, \rho E, \rho\phi) \right|_{\rho, \rho v, \rho\phi} = \frac{P_e(\rho, e, \rho\phi)}{\rho} \\ \left. \frac{\partial \bar{P}}{\partial \rho\phi}(\rho, \rho v, \rho E, \rho\phi) \right|_{\rho, \rho v, \rho E} &= \left. \frac{\partial P}{\partial \rho\phi}(\rho, e, \rho\phi) \right|_{\rho, e}. \end{aligned} \quad (30)$$

For brevity, we introduce the following short-hand notation: $\bar{P}_\rho : \mathbb{R}_{\geq 0} \times \mathbb{R}^{d'} \times \mathbb{R} \times \mathbb{R}_{\geq 0} \rightarrow \mathbb{R}$, $\bar{P}_{\rho v} : \mathbb{R}_{\geq 0} \times \mathbb{R}^{d'} \times \mathbb{R} \times \mathbb{R}_{\geq 0} \rightarrow \mathbb{R}^{d'}$, $\bar{P}_{\rho E} : \mathbb{R}_{\geq 0} \times \mathbb{R}^{d'} \times \mathbb{R} \times \mathbb{R}_{\geq 0} \rightarrow \mathbb{R}$, defined as

$$\begin{aligned} \bar{P}_\rho : (\rho, \rho v, \rho E, \rho\phi) &\mapsto \left. \frac{\partial \bar{P}}{\partial \rho}(\rho, \rho v, \rho E, \rho\phi) \right|_{\rho v, \rho E, \rho\phi}, \\ \bar{P}_{\rho v} : (\rho, \rho v, \rho E, \rho\phi) &\mapsto \left. \frac{\partial \bar{P}}{\partial \rho v}(\rho, \rho v, \rho E, \rho\phi) \right|_{\rho, \rho E, \rho\phi}, \\ \bar{P}_{\rho E} : (\rho, \rho v, \rho E, \rho\phi) &\mapsto \left. \frac{\partial \bar{P}}{\partial \rho E}(\rho, \rho v, \rho E, \rho\phi) \right|_{\rho, \rho v, \rho\phi}, \\ \bar{P}_{\rho\phi} : (\rho, \rho v, \rho E, \rho\phi) &\mapsto \left. \frac{\partial \bar{P}}{\partial \rho\phi}(\rho, \rho v, \rho E, \rho\phi) \right|_{\rho, \rho v, \rho E}. \end{aligned} \quad (31)$$

From these definitions, the spatial projected inviscid Jacobian for the two-phase Euler equations with general equations of state is

$$B_x : (U_x, \eta_x) \mapsto \begin{bmatrix} 0 & \eta_x^T & 0 & 0 \\ -v_n v + \bar{P}_\rho \eta_x & v_n I_{d'} + v \eta_x^T + \eta_x \bar{P}_{\rho v}^T & \bar{P}_{\rho E} \eta_x & \bar{P}_{\rho\phi} \eta_x \\ (\bar{P}_\rho - H) v_n & H \eta_x^T + v_n \bar{P}_{\rho v}^T & (1 + \bar{P}_{\rho E}) v_n & \bar{P}_{\rho\phi} v_n \\ -\phi v_n & \phi \eta_x^T & 0 & v_n \end{bmatrix}, \quad (32)$$

which, using (30), simplifies to

$$B_x : (U_x, \eta_x) \mapsto \begin{bmatrix} 0 & \eta_x^T & 0 & 0 \\ -v_n v + \bar{P}_\rho \eta_x & v_n I_{d'} + v \eta_x^T - \frac{P_e}{\rho} \eta_x v^T & \frac{P_e}{\rho} \eta_x & \bar{P}_{\rho\phi} \eta_x \\ (\bar{P}_\rho - H) v_n & H \eta_x^T - v_n \frac{P_e}{\rho} v^T & (1 + \frac{P_e}{\rho}) v_n & \bar{P}_{\rho\phi} v_n \\ -\phi v_n & \phi \eta_x^T & 0 & v_n \end{bmatrix} \quad (33)$$

where $\eta_x \in \mathbb{R}^{d'}$ is the unit normal, $v_n := v \cdot \eta_x$, and $I_{d'}$ is the $d' \times d'$ identity matrix. The matrix of right eigenvectors is given by

$$V_x : (U_x, \eta_x) \mapsto \begin{bmatrix} 1 & \eta_x^T & 0 & 1 \\ v - c\eta_x & (v - \eta_x)\eta_x^T + I_{d'} & 0 & v + c\eta_x \\ H - v_n c & v^T + (\theta - v_n)\eta_x^T & -\bar{P}_{\rho\phi} & H + v_n c \\ \phi & \vec{0}^T & \frac{P_e}{\rho} & \phi \end{bmatrix}, \quad (34)$$

where θ is defined in (23) and the sound speed, c , is defined as

$$c^2 = \bar{P}_\rho + (H - \|v\|^2) \frac{P_e}{\rho} + \phi P_{\rho\phi}. \quad (35)$$

Derivation of the (35) is provided in Appendix B.2. The diagonal matrix of eigenvalues corresponding to these right eigenvectors is

$$\Lambda_x : (U_x, \eta_x) \mapsto \begin{bmatrix} v_n - c & 0 & 0 & 0 \\ 0 & v_n I_{d'} & 0 & 0 \\ 0 & 0 & v_n & 0 \\ 0 & 0 & 0 & v_n + c \end{bmatrix} \quad (36)$$

Finally, the matrix of left eigenvectors is given by

$$V^{-1} : (U_x, \eta_x) \mapsto \frac{1}{2c^2\rho} \begin{bmatrix} \rho\bar{P}_\rho + c\rho v_n & -c\rho\eta_x^T - P_e v^T & P_e & \bar{P}_{\rho\phi}\rho \\ 2c^2\rho(\eta_x v_n - v) + 2\eta_x \omega & 2c^2\rho(I_{d'} - \eta_x \eta_x^T) + 2P_e \eta_x v^T & -2\eta_x P_e & -2\rho\bar{P}_{\rho\phi}\eta_x \\ \frac{-2\phi\bar{P}_\rho\rho^2}{P_e} & 2\phi\rho v^T & 2\phi\rho & \frac{2\rho\omega}{P_e} \\ \rho\bar{P}_\rho - c\rho v_n & c\rho\eta_x^T - P_e v^T & P_e & \bar{P}_{\rho\phi}\rho \end{bmatrix} \quad (37)$$

where $\omega = (HP_e - P_e\|v\|^2 + \rho\phi\bar{P}_{\rho\phi})$.

2.6. Two-phase mixture equation of state

Recall from Section 1 that the method proposed in this manuscript is a *sharp-interface* model for two-phase flow; the phase-field formulation is used as a means to converge to the sharp interface, i.e., $\phi(x, t) \in \{0, 1\}$ using implicit shock tracking. As such, the requirements on our mixture model are much weaker than most phase-field models where $\phi(x, t) \in [0, 1]$ and require thermodynamic consistency in mixture regions, i.e., $(x, t) \in \Omega_x \times \mathcal{T}$ such that $0 < \phi(x, t) < 1$ [64]. In our setting, we only require the mixture model is consistent in the sense that all thermodynamic properties (e.g., pressure and sound speed) reduce to that of the individual fluids as $\phi \rightarrow 0, 1$, e.g., in the case of pressure,

$$\lim_{\phi \rightarrow 1} P(\rho, e, \rho\phi) = P_1(\rho, e), \quad \lim_{\phi \rightarrow 0} P(\rho, e, \rho\phi) = P_2(\rho, e), \quad (38)$$

where $P_1(\rho, e)$ and $P_2(\rho, e)$ are the equations of state of the two fluids under consideration. No requirements are imposed on mixtures $0 < \phi < 1$. Thus, we choose the simplest mixture model

$$P(\rho, e, \rho\phi) = \frac{\rho\phi}{\rho} P_1(\rho, e) + \left(1 - \frac{\rho\phi}{\rho}\right) P_2(\rho, e) \quad (39)$$

which clearly satisfies (38) and the sound speed also approaches the material truths as $\phi \rightarrow 0, 1$ (derivation in Appendix B.3).

The partial derivatives of P are needed to define the inviscid projected Jacobian and eigenvalue decompositions of the two-phase Euler equations (Section 2.5). First, the partial derivative with respect to density, $P_\rho(\rho, e, \rho\phi)$, is

$$\begin{aligned} P_\rho(\rho, e, \rho\phi) &= \frac{\partial}{\partial \rho} \left(\frac{\rho\phi}{\rho} P_1(\rho, e) + \left(1 - \frac{\rho\phi}{\rho}\right) P_2(\rho, e) \right) \\ &= \frac{\phi}{\rho} (P_2(\rho, e) - P_1(\rho, e)) + \phi \left(\left. \frac{\partial P_1}{\partial \rho}(\rho, e) \right|_e - \left. \frac{\partial P_2}{\partial \rho}(\rho, e) \right|_e \right) + \left. \frac{\partial P_2}{\partial \rho}(\rho, e) \right|_e. \end{aligned} \quad (40)$$

The partial derivative with respect to internal energy, $P_e(\rho, e, \rho\phi)$, is

$$\begin{aligned} P_e(\rho, e, \rho\phi) &= \frac{\partial}{\partial e} \left(\frac{\rho\phi}{\rho} P_1(\rho, e) + \left(1 - \frac{\rho\phi}{\rho}\right) P_2(\rho, e) \right) \\ &= \phi \frac{\partial P_1}{\partial e}(\rho, e) \Big|_{\rho} + (1 - \phi) \frac{\partial P_2}{\partial e}(\rho, e) \Big|_{\rho} \end{aligned} \quad (41)$$

Finally, the partial derivative with respect to the phase, $P_{\rho\phi}(\rho, e, \rho\phi)$, is

$$P_{\rho\phi}(\rho, e, \rho\phi) = \frac{\partial}{\partial \rho\phi} \left(\frac{\rho\phi}{\rho} P_1(\rho, e) + \left(1 - \frac{\rho\phi}{\rho}\right) P_2(\rho, e) \right) = \frac{P_1 - P_2}{\rho} \quad (42)$$

From these three expressions, all terms in Section 2.5 are well-defined once an equation of state is selected for each fluid (Section 2.7).

Remark 1. *In the special case where both fluids are identical, i.e., $P_1(\rho, e) = P_2(\rho, e)$, the mixture equation of state (39) and its partial derivatives (39)-(42) are independent of ϕ .*

2.7. Equations of state considered

In this section we outline the equations of state considered (Section 5) in the notation of Section 2.4. In particular, we consider an ideal gas (Section 2.7.1), a stiffened gas model of water (Section 2.7.2), and the Becker-Kistiakowsky-Wilson (BKW) equation of state [8, 31, 38, 62, 41] used to model gaseous byproducts in detonations (Section 2.7.3). These single-phase real gas equations of state are used to construct the two-phase mixture equation of state (39) in Section 2.6.

2.7.1. Ideal gas

First, we introduce an ideal gas using the formalism of Section 2.4 as a simple demonstration and validation case in Section 5. An ideal gas is calorically perfect with equation of state

$$P^{IG}(\rho, e) = (\gamma - 1)\rho e, \quad (43)$$

where $\gamma > 1$ is the ratio of specific heats. The ideal gas can also be written in terms of temperature, $T^{IG} : \mathbb{R}_{\geq 0} \rightarrow \mathbb{R}_{\geq 0}$, as

$$P^{IG}(\rho, e) = \rho R T^{IG}(e), \quad (44)$$

where $R \in \mathbb{R}_{> 0}$ is the universal gas constant and $T^{IG} : e \mapsto (\gamma - 1)e/R$. The partial derivatives of this equation of state are

$$P_{\rho}^{IG}(\rho, e) = (\gamma - 1)e, \quad P_e^{IG}(\rho, e) = (\gamma - 1)\rho. \quad (45)$$

The equations for the projected flux Jacobian (21) and its eigenvalue decomposition (22)-(26) reduce to their usual definitions for an ideal gas [40] if (43)-(45) are substituted for P , P_{ρ} , and P_e (Appendix A).

2.7.2. Stiffened gas

Next, we introduce stiffened gas model of water [3] with equation of state

$$P^{SG}(\rho, e) = (\gamma - 1)\rho e - \gamma P^*, \quad (46)$$

where P^* is a constant representing the molecular attraction between water molecules. In terms of temperature, $T^{SG} : \mathbb{R}_{\geq 0} \times \mathbb{R}_{\geq 0} \rightarrow \mathbb{R}_{\geq 0}$, the stiffened gas equation of state is

$$P^{SG}(\rho, e) = \rho R T^{SG}(\rho, e) Z^{SG}(\rho, e), \quad (47)$$

where $T^{SG} : (\rho, e) \mapsto (e - P^*/\rho)/C_V$, $Z^{SG} : (\rho, e) \mapsto 1 - P^*/(\rho R T^{SG}(\rho, e))$ is the compressibility factor, and $C_V \in \mathbb{R}_{\geq 0}$ is specific heat at constant volume. Because this stiffened gas model is just an ideal gas law with an additional constant term, its partial derivatives are the identical to those of the ideal gas equation of state, i.e.,

$$P_{\rho}^{SG}(\rho, e) = (\gamma - 1)e, \quad P_e^{SG}(\rho, e) = (\gamma - 1)\rho. \quad (48)$$

2.7.3. Becker-Kistiakowsky-Wilson (BKW) equation of state

The Becker-Kistiakowsky-Wilson (BKW) equation of state is often used as a simplified model of the gaseous byproduct from a detonation [8, 31, 38, 62, 41] and takes the form

$$P^{BKW}(\rho, e) = \hat{P}^{BKW}(\rho, T^{BKW}(\rho, e)), \quad \hat{P}^{BKW}(\rho, T) = \rho RT \hat{Z}^{BKW}(\rho, T), \quad (49)$$

where the compressibility factor, $\hat{Z}^{BKW} : \mathbb{R}_{\geq 0} \times \mathbb{R}_{\geq 0} \rightarrow \mathbb{R}$, is defined as

$$\hat{Z}^{BKW} : (\rho, T) \mapsto (1 + \hat{X}(\rho, T) \exp(\beta \hat{X}(\rho, T))), \quad (50)$$

the function $\hat{X} : \mathbb{R}_{\geq 0} \times \mathbb{R}_{\geq 0} \rightarrow \mathbb{R}$ is defined as

$$\hat{X} : (\rho, T) \mapsto \frac{\kappa \rho}{(T + \theta)^\alpha}, \quad (51)$$

and $\beta, \kappa, \theta, \alpha$ are all scalar constants. The temperature, $T^{BKW} : \mathbb{R}_{\geq 0} \times \mathbb{R}_{\geq 0} \rightarrow \mathbb{R}_{\geq 0}$, $T^{BKW} : (\rho, e) \mapsto T^{BKW}(\rho, e)$, is implicitly defined as the solution (T) of the nonlinear scalar equation (given ρ and e)

$$e^{BKW}(\rho, T) = e, \quad (52)$$

which must be solved using nonlinear iterations. For this equation of state, the internal energy, $e^{BKW} : \mathbb{R}_{\geq 0} \times \mathbb{R}_{\geq 0} \rightarrow \mathbb{R}_{\geq 0}$, is defined in terms of the density and temperature as

$$e^{BKW} : (\rho, T) \mapsto \frac{\alpha RT^2 X(\rho, T) \exp(\beta X(\rho, T))}{T + \theta} + aT^2 + bT + c, \quad (53)$$

where a, b, c are constant coefficients calibrated to the gas under consideration.

Recall, the partial derivatives of the equation of state are crucial to define the conservation law flux and its Jacobian (Section 2.4). The partial derivatives of the BKW equation of state are

$$\begin{aligned} P_\rho^{BKW}(\rho, e) &= \left. \frac{\partial \hat{P}^{BKW}}{\partial \rho}(\rho, T^{BKW}(\rho, e)) \right|_T + \left. \frac{\partial \hat{P}^{BKW}}{\partial T}(\rho, T^{BKW}(\rho, e)) \right|_\rho \left. \frac{\partial T^{BKW}}{\partial \rho}(\rho, e) \right|_e \\ P_e^{BKW}(\rho, e) &= \left. \frac{\partial \hat{P}^{BKW}}{\partial T}(\rho, T^{BKW}(\rho, e)) \right|_\rho \left. \frac{\partial T^{BKW}}{\partial e}(\rho, e) \right|_\rho. \end{aligned} \quad (54)$$

Both of the derivatives depend on derivatives of T^{BKW} , which is implicitly defined as the solution of the nonlinear equation in (52). To derive these derivatives, introduce a new function, $F : \mathbb{R}_{\geq 0} \times \mathbb{R}_{\geq 0} \rightarrow \mathbb{R}$, defined as

$$F(\rho, e) = e^{BKW}(\rho, T^{BKW}(\rho, e)) - e. \quad (55)$$

From (52), F is the zero function, which means $\frac{\partial F}{\partial \rho}(\rho, e) = \frac{\partial F}{\partial e}(\rho, e) = 0$ for any $\rho, e \in \mathbb{R}_{\geq 0}$. Equation (55) and the fact that the derivatives of F are zero leads to the following equations

$$\begin{aligned} \frac{\partial F}{\partial \rho}(\rho, e) &= \left. \frac{\partial e^{BKW}}{\partial \rho}(\rho, T^{BKW}(\rho, e)) \right|_T + \left. \frac{\partial e^{BKW}}{\partial T}(\rho, T^{BKW}(\rho, e)) \right|_\rho \left. \frac{\partial T^{BKW}}{\partial \rho}(\rho, e) \right|_e = 0 \\ \frac{\partial F}{\partial e}(\rho, e) &= \left. \frac{\partial e^{BKW}}{\partial T}(\rho, T^{BKW}(\rho, e)) \right|_\rho \left. \frac{\partial T^{BKW}}{\partial e}(\rho, e) \right|_\rho - 1 = 0 \end{aligned} \quad (56)$$

These equations can easily be solved for the unknown partial derivatives to yield

$$\begin{aligned} \left. \frac{\partial T^{BKW}}{\partial \rho}(\rho, e) \right|_e &= - \left[\left. \frac{\partial e^{BKW}}{\partial T}(\rho, T^{BKW}(\rho, e)) \right|_\rho \right]^{-1} \left. \frac{\partial e^{BKW}}{\partial \rho}(\rho, T^{BKW}(\rho, e)) \right|_T \\ \left. \frac{\partial T^{BKW}}{\partial e}(\rho, e) \right|_\rho &= \left[\left. \frac{\partial e^{BKW}}{\partial T}(\rho, T^{BKW}(\rho, e)) \right|_\rho \right]^{-1} \end{aligned} \quad (57)$$

after $T^{BKW}(\rho, e)$ has been obtained from the solution of (52). All partial derivatives of e^{BKW} can be derived analytically from (53).

Remark 2. In practice, the nonlinear equation (52) must be solved many times, e.g., at every quadrature node of every element of the finite element mesh (Section 3), for a single discrete residual or Jacobian evaluation, so efficiency of the nonlinear solver is paramount. We use Newton's method due to its quadratic convergence with a linear model to determine the initial guess. In particular, given $\rho, e \in \mathbb{R}_{\geq 0}$ (input to the nonlinear system), we construct a linear model of the form $\tilde{T}(\tilde{e}) = a + b\tilde{e}$ with constants a, b defined such that $\tilde{T}(e^{BKW}(\rho, T_1)) = T_1$ and $\tilde{T}(e^{BKW}(\rho, T_2)) = T_2$, where $T_1, T_2 \in \mathbb{R}_{\geq 0}$ are estimates of the extreme values of temperature encountered during the problem. Then, the nonlinear iterations are initialized with $T^{(0)} = \tilde{T}(e)$. For all problems considered in this work (Section 5), we use $T_1 = 10K$ and $T_2 = 3000K$.

3. Discontinuous Galerkin discretization of the transformed space-time conservation law

We discretize the transformed conservation law (11) with a discontinuous Galerkin method [21] with high-order piecewise polynomials spaces used to approximate the state \bar{U} and domain mapping \mathcal{G} . To this end, let $\bar{\mathcal{E}}_h$ represent a discretization of the reference domain Ω_0 into non-overlapping, potentially curved, computational elements. To establish the finite-dimensional DG formulation, we introduce the DG approximation (trial) space of discontinuous piecewise polynomials associated with the mesh $\bar{\mathcal{E}}_h$

$$\mathcal{V}_h^p := \{v \in [L^2(\bar{\Omega})]^m \mid v|_{\bar{K}} \in [\mathcal{P}_p(\bar{K})]^m, \forall \bar{K} \in \bar{\mathcal{E}}_h\}, \quad (58)$$

where $\mathcal{P}_p(\bar{K})$ is the space of polynomial functions of degree at most $p \geq 0$ over the domain \bar{K} . Furthermore, we define the space of globally continuous piecewise polynomials of degree q associated with the mesh $\bar{\mathcal{E}}_h$ as

$$\mathcal{W}_h := \{v \in C^0(\bar{\Omega}) \mid v|_{\bar{K}} \in \mathcal{P}_q(\bar{K}), \forall \bar{K} \in \bar{\mathcal{E}}_h\} \quad (59)$$

and discretize the domain mapping with the corresponding vector-valued space $[\mathcal{W}_h]^d$. With these definitions, the DG variational problem is: given $\mathcal{G}_h \in [\mathcal{W}_h]^d$, find $\bar{U}_h \in \mathcal{V}_h^p$ such that for all $\bar{\psi}_h \in \mathcal{V}_h^{p'}$, we have

$$r_h^{p',p}(\bar{\psi}_h, \bar{U}_h; \bar{\nabla} \mathcal{G}_h) = 0 \quad (60)$$

where $p' \geq p$ and the global residual function $r_h^{p',p} : \mathcal{V}_h^{p'} \times \mathcal{V}_h^p \times [\mathcal{W}_h]^d \rightarrow \mathbb{R}$ is defined in terms of elemental residuals $r_{\bar{K}}^{p',p} : \mathcal{V}_h^{p'} \times \mathcal{V}_h^p \times [\mathcal{W}_h]^d \rightarrow \mathbb{R}$ as

$$r_h^{p',p} : (\bar{\psi}_h, \bar{W}_h; \Theta_h) \mapsto \sum_{\bar{K} \in \bar{\mathcal{E}}_h} r_{\bar{K}}^{p',p}(\bar{\psi}_h, \bar{W}_h; \Theta_h). \quad (61)$$

The elemental residuals come directly from a standard DG formulation applied to the transformed space-time conservation law in (11)

$$\begin{aligned} r_{\bar{K}}^{p',p} : (\bar{\psi}_h, \bar{W}_h; \Theta_h) \mapsto & \int_{\partial \bar{K}} \bar{\psi}_h \cdot \bar{\mathcal{H}}(W_h^+, W_h^-, \bar{\eta}_h; \Theta_h) dS \\ & - \int_{\bar{K}} \bar{\mathcal{F}}(W_h; \Theta_h) : \bar{\nabla} \bar{\psi}_h dV \\ & - \int_{\bar{K}} \bar{\psi}_h \cdot \bar{\mathcal{S}}(W_h; \det \Theta_h) dV, \end{aligned} \quad (62)$$

where $\bar{\eta}_h : \partial \bar{K} \mapsto \mathbb{R}^d$ is the outward unit normal to an element $\bar{K} \in \bar{\mathcal{E}}_h$, \bar{W}_h^+ (\bar{W}_h^-) denotes the interior (exterior) trace of $\bar{W}_h \in \mathcal{V}_h^p$ to the element, and $\bar{\mathcal{H}}$ is the transformed space-time numerical (Roe) flux function [51].

Following the approach in [74, 40], we define the transformed numerical flux function, $\bar{\mathcal{H}} : \mathbb{R}^m \times \mathbb{R}^m \times \mathbb{S}_d \times \mathbb{R}^{d \times d} \mapsto \mathbb{R}^m$, as

$$\bar{\mathcal{H}} : (\bar{W}^+, \bar{W}^-, \bar{\eta}; \Theta) \mapsto \sigma \mathcal{H}(\bar{W}^+, \bar{W}^-, \sigma^{-1}(\det \Theta) \Theta^{-T} \bar{\eta}) \quad (63)$$

where $\sigma = \|(\det \Theta) \Theta^{-T} \bar{\eta}\|$ is defined for brevity and $\mathcal{H} : \mathbb{R}^m \times \mathbb{R}^m \times \mathbb{S}_d \rightarrow \mathbb{R}^m$ is the space-time numerical flux, defined as [40]

$$\mathcal{H} : (W^+, W^-, \eta) \mapsto \frac{1}{2} (\mathcal{F}(W^+) \eta + \mathcal{F}(W^-) \eta) + \frac{1}{2} \tilde{B}(W^+, W^-, \eta) (W^+ - W^-). \quad (64)$$

The Jacobian of the linearized Riemann problem $\tilde{B} : \mathbb{R}^m \times \mathbb{R}^m \times \mathbb{S}_d \rightarrow \mathbb{R}^{m \times m}$ is

$$\tilde{B}(W^+, W^-, \eta) = \left| B(\hat{U}(W^+, W^-), \eta) \right|, \quad (65)$$

which can be directly written in terms of spatial quantities using (10)

$$\tilde{B}(W^+, W^-, \eta) = V_x(\hat{W}, \eta_x) \left| \Lambda_x(\hat{W}, \eta_x) \|n_x\| + n_t I_m \right| V_x(\hat{W}, \eta_x)^{-1}, \quad (66)$$

where $\hat{W} = \hat{U}(W^+, W^-)$ was introduced for brevity and $\hat{U} : \mathbb{R}^m \times \mathbb{R}^m \rightarrow \mathbb{R}^m$ is the equation-specific Roe average (Appendix C).

Finally, we introduce a basis for the test space ($\mathcal{V}_h^{p'}$), trial space (\mathcal{V}_h^p), and domain mapping space ($[\mathcal{W}_h]^d$) to reduce the weak formulation in (60)-(62) to a system of nonlinear algebraic equations. In the case where $p = p'$, we have

$$\mathbf{r} : \mathbb{R}^{N_u} \times \mathbb{R}^{N_x} \rightarrow \mathbb{R}^{N_u}, \quad \mathbf{r} : (\mathbf{u}, \mathbf{x}) \mapsto \mathbf{r}(\mathbf{u}, \mathbf{x}), \quad (67)$$

where $N_u = \dim(\mathcal{V}_h^p)$ and $N_x = \dim([\mathcal{W}_h]^d)$, which is the residual of a standard space-time DG method. Furthermore, we define the algebraic enriched residual associated with a test space of degree $p' > p$ ($p' = p + 1$ in this work) as

$$\mathbf{R} : \mathbb{R}^{N_u} \times \mathbb{R}^{N_x} \rightarrow \mathbb{R}^{N'_u}, \quad \mathbf{R} : (\mathbf{u}, \mathbf{x}) \mapsto \mathbf{R}(\mathbf{u}, \mathbf{x}), \quad (68)$$

where $N'_u = \dim(\mathcal{V}_h^{p'})$, which will be used to construct the implicit shock tracking objective function.

4. Implicit shock tracking for two-phase flow

In this section we formulate the implicit shock tracking optimization problem for two-phase flow (Section 4.1) using the machinery established in Sections 2-3 and review important details of implicit shock tracking for space-time problems (Section 4.2) from [40].

4.1. Formulation

Let $\phi : \mathbb{R}^{N_y} \rightarrow \mathbb{R}^{N_x}$, $\phi : \mathbf{y} \mapsto \phi(\mathbf{y})$ be a boundary-preserving parametrization of the mesh nodal coordinate $\mathbf{x} \in \mathbb{R}^{N_x}$, where $\mathbf{y} \in \mathbb{R}^{N_y}$ is a vector of unconstrained degrees of freedom, i.e., for any $\mathbf{y} \in \mathbb{R}^{N_y}$, then $\mathbf{x} = \phi(\mathbf{y})$ are nodal coordinates that preserve all boundaries of the computational domain [74, 22, 40]. The HOIST method is formulated as an optimization problem over the DG solution coefficients and the unconstrained mesh degrees of freedom

$$(\mathbf{u}^*, \mathbf{y}^*) := \arg \min_{\mathbf{u} \in \mathbb{R}^{N_u}, \mathbf{y} \in \mathbb{R}^{N_y}} f(\mathbf{u}, \phi(\mathbf{y})) \quad \text{subject to: } \mathbf{r}(\mathbf{u}, \phi(\mathbf{y})) = \mathbf{0}, \quad (69)$$

where $f : \mathbb{R}^{N_u} \times \mathbb{R}^{N_x} \rightarrow \mathbb{R}$ is the objective function defined in [74, 22]. The objective function is composed of two terms as

$$f : (\mathbf{u}, \mathbf{x}) \mapsto f_{\text{err}}(\mathbf{u}, \mathbf{x}) + \kappa^2 f_{\text{msh}}(\mathbf{x}), \quad (70)$$

which balances alignment of the mesh with non-smooth features and the quality of the elements, and κ is the mesh penalty parameter. The mesh alignment term (f_{err}) is taken to be the norm of the enriched DG residual

$$f_{\text{err}} : (\mathbf{u}, \mathbf{x}) \rightarrow \frac{1}{2} \|\mathbf{R}(\mathbf{u}, \mathbf{x})\|_2^2, \quad (71)$$

which promotes mesh alignment by penalizing non-physical oscillations that arise on meshes that are not discontinuity-aligned. The mesh quality term (f_{msh}) is a measure of the element-wise mesh distortion [22]. A sequential quadratic programming (SQP) method, globalized with a line search on the ℓ_1 merit function, is used to solve the optimization problem in (69) by simultaneously converging (\mathbf{u}, \mathbf{x}) to their optimal values $(\mathbf{u}^*, \mathbf{x}^*)$. The parameter $\kappa \in \mathbb{R}$, which balances the contributions of the shock tracking and mesh quality terms, is adapted during the SQP iterations using the algorithm described in [22]. For a complete description of the HOIST method and SQP solver, the reader is referred to [74, 22].

4.2. Space-time implicit shock tracking

In this work, we solve time-dependent two-phase flow using the space-time HOIST method [40]. The transformed space-time conservation law (11) is discretized in space-time resulting in a $(d' + 1)$ -dimensional conservation law (Sections 2.1-2.2). To avoid coupling the entire temporal domain, the time domain is partitioned, which creates smaller, more manageable space-time *slabs*. The HOIST method (Section 4.1) is applied sequentially over individual slabs to align the space-time slab mesh with discontinuities and compute the corresponding flow solution. After the aligned mesh and flow solution are available on a given slab, a space-time mesh of the next slab is formed by (1) extracting the upper temporal boundary, a d' -dimensional mesh, from the current slab, (2) extruding the d' -dimensional to form space-time prisms, and (3) splitting the prisms into space-time simplices [40]. This process ensures the lower temporal boundary (initial time) of the mesh of any slab conforms to the upper temporal boundary (final time) of the mesh of the previous slab. As a result, the lower temporal boundary of the mesh of any slab is aligned with discontinuities so we choose to freeze the nodes on the lower temporal boundary using the mesh parametrization ϕ . The initial condition of each slab (boundary condition on the lower temporal boundary) is obtained by transferring the solution on the upper temporal boundary of previous slab to the quadrature nodes on the lower temporal boundary of the current slab mesh. This procedure repeats until the union of all the slabs covers the entire temporal domain of interest. A complete description of the space-time HOIST method can be found in [40].

Many two-phase flows, particularly the blast problems considered in this work, have huge disparities in the spatial and temporal scales. This can lead to space-time meshes with excessive resolution in either the spatial or temporal dimension or highly skewed meshes. To avoid this, we nondimensionalize the time-dependent conservation law (2) by introducing a spatial L^* , temporal t^* , and mass m^* scaling, and reformulating (2) in terms of nondimensional quantities [40]. These scales are chosen such that: 1) the components of the solution vector (U_x) have similar magnitudes to improve the conditioning/scaling of the optimization problem in (69) and 2) the spatial and temporal dimensions have similar magnitudes, which ensures the space-time meshes are well-conditioned using the extract-extrude-split approach above. The specific scales for different problems in the numerical experiments (Section 5) are noted in the problem description.

5. Numerical experiments

In this section, we apply the slab-based HOIST method to a range of two-phase flow Riemann problems. We begin with a single-phase, ideal gas validation of the real gas two-phase framework of Section 2 to demonstrate it recovers this limiting case (Section 5.1). Next, we present a two-phase validation where both fluids are ideal gases with different γ values (Section 5.2) and an ideal-stiffened gas validation (Section 5.3). Finally, demonstrate the framework on a spherically symmetric underwater explosion where the gas is modeled with the BKW equation of state and water is modeled as a stiffened gas (Section 5.4).

5.1. Sod's shock tube: single-phase, ideal gas validation

Sod's shock tube is a Riemann problem for the Euler equations that models an idealized shock tube where the membrane separating a high pressure region from a low pressure one is instantaneously removed. This is a commonly used validation problem because it has an analytical solution that features a shock wave, rarefaction wave, and contact discontinuity. This problem serves as a simple validation of the two-phase real gas HOIST method in the single-phase, ideal gas limit.

We model Sod's shock tube using the two-phase real gas framework of Section 2, i.e., the two-phase Euler equations (2) and (27) with mixture equation of state (39). Both fluids are taken to be ideal gases with the same ratio of specific heats $\gamma_1 = \gamma_2 = 7/5$, thus reducing to a single-phase, ideal gas flow. We consider the space-time domain $\Omega_x := (0, 1)$ and $\mathcal{T} = (0, 0.1]$ with initial condition

$$\rho(x, 0) = \begin{cases} 1 & x < 0.5 \\ 0.125 & x \geq 0.5 \end{cases}, \quad v(x, 0) = 0, \quad P(x, 0) = \begin{cases} 1 & x < 0.5 \\ 0.1 & x \geq 0.5 \end{cases}, \quad \phi(x, 0) = \begin{cases} 1 & x < 0.5 \\ 0 & x \geq 0.5 \end{cases} \quad (72)$$

Because both fluids are identical, the mixture equation of state (39) is independent of ϕ (Remark 1), which makes $\phi(x, t)$ arbitrary. The solution of this problem contains three waves (shock, contact, rarefaction) that emanate from $x = 0.5$ at $t = 0$.

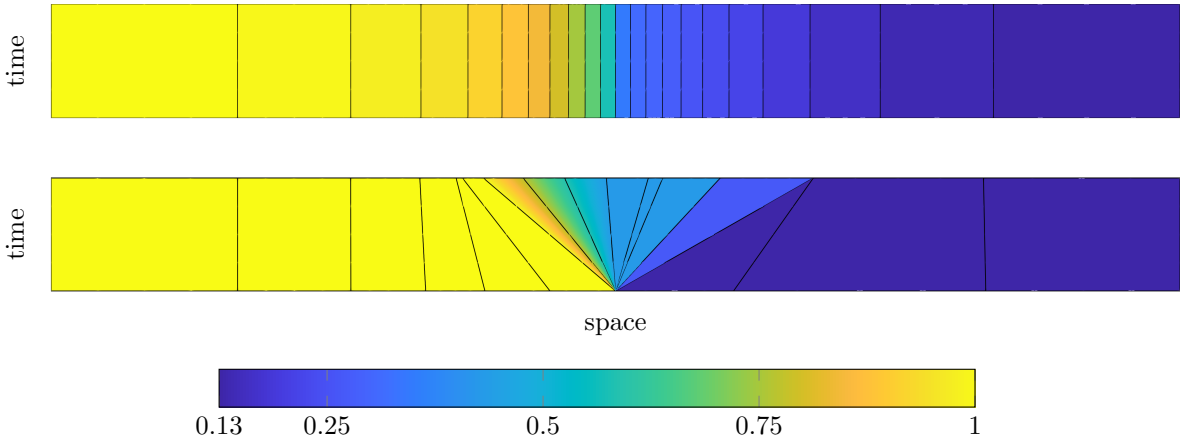


Figure 3: Two-phase HOIST solution (density) for single-phase, ideal gas Sod shock tube problem using one slab (*bottom*) and the mesh and solution used to initialize the HOIST solver (*top*).

A single time slab is used to cover the entire time domain with an initial (non-aligned) space-time mesh consisting of 22 linear ($q = 1$) quadrilateral elements with quadratic ($p = 2$) solution approximation over each. The problem is nondimensionalized using the scalings $L^* = t^* = m^* = 1$ because the spatial and temporal scales are similar magnitudes. The HOIST solver is initialized from the $p = 0$ DG solution on the initial space-time mesh (Figure 3). The final HOIST solution has tracked the lead shock, contact discontinuity, and the head and tail of the rarefaction (Figure 3). Furthermore, the HOIST solution shows near perfect agreement with the analytical solution to this problem at $t = 0.1$ (Figure 4 (*left*)).

To close this section, we perform a mesh convergence study of the HOIST method for this problem (Figure 4 (*right*)), which confirms the method achieves the optimal convergence, $\mathcal{O}(h^{p+1})$, for $p = 2$. The error is measured using the L^1 -norm of density at the final time $t = 0.1$ against the analytical solution, i.e.,

$$E_h : h \mapsto \int_0^1 |\rho(x, 0.1) - \rho_h(x, 0.1)| dx, \quad (73)$$

where $\rho(x, t)$ is the analytical solution and $\rho_h(x, t)$ is the HOIST solution on the mesh with grid measure (longest edge in mesh) h . We use the L^1 error because it is expected to converge at the optimal rate for discontinuous solutions provided the smooth solution and position of the discontinuity converge at that rate [22, 74].

5.2. Sod's shock tube: two-phase, ideal gas validation

Next, we apply our method to a variation of Sod's shock tube involving two different ideal gases to validate the two-phase HOIST method in this limiting case. In particular, the high-pressure region is an ideal gas with $\gamma_1 = 7/5$ and the low-pressure region is an ideal gas with $\gamma_2 = 7/3$. We consider the space-time domain $\Omega_x := (0, 1)$ and $\mathcal{T} = (0, 0.1]$ with initial condition

$$\rho(x, 0) = \begin{cases} 1 & x < 0.5 \\ 0.125 & x \geq 0.5 \end{cases}, \quad v(x, 0) = 0, \quad P(x, 0) = \begin{cases} 1 & x < 0.5 \\ 0.1 & x \geq 0.5 \end{cases}, \quad \phi(x, 0) = \begin{cases} 1 & x < 0.5 \\ 0 & x \geq 0.5 \end{cases}. \quad (74)$$

We use the convention defined in (39) that $\phi(x, t) = 1$ indicates material 1 occupies $(x, t) \in \Omega_x \times \mathcal{T}$, and material 2 occupies any $(x, t) \in \Omega_x \times \mathcal{T}$ where $\phi(x, t) = 0$. The solution of this problem contains three waves (shock, contact, rarefaction) that emanate from $x = 0.5$ at $t = 0$.

A single slab is used to cover the entire time domain with an initial (non-aligned) space-time mesh consisting of 22 linear ($q = 1$) quadrilateral elements with quadratic ($p = 2$) solution approximation over

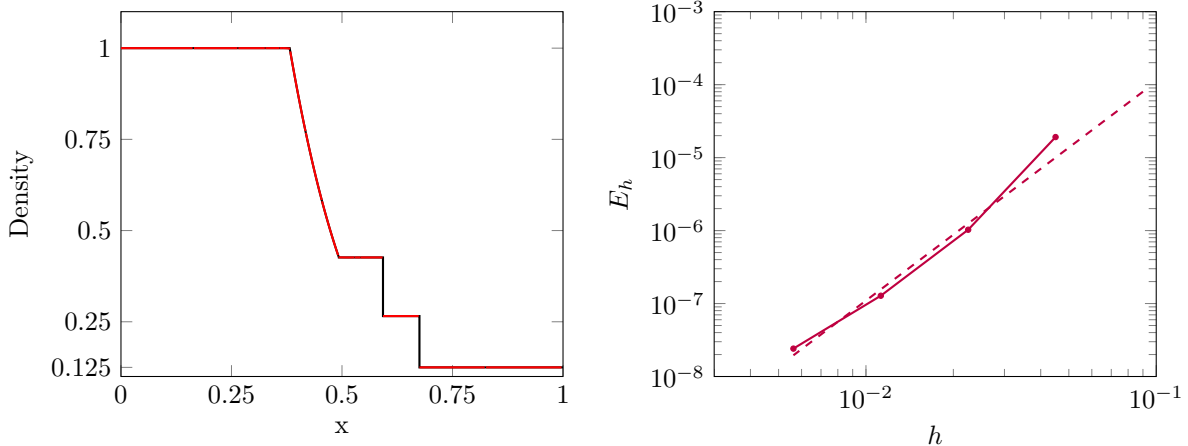


Figure 4: *Left*: Slice of two-phase HOIST solution (density) (—) to the single-phase, ideal gas Sod shock tube problem at the final time, and the corresponding analytical solution (—). *Right*: Mesh convergence of the two-phase HOIST method ($p = 2$) applied to the single-phase Sod shock tube problem measured using L^1 error at time $t = 0.1$. Legend (*right*): HOIST solution error (—•) and optimal convergence rate ($p + 1$) (---).

each. The problem is nondimensionalized using the scalings $L^* = t^* = m^* = 1$ because the spatial and temporal scales are similar magnitudes. The HOIST solver is initialized from the $p = 0$ DG solution on the initial space-time mesh. As the SQP iterations proceed, the faces of the mesh are driven towards alignment with the lead shock, contact discontinuity, and head and tail of the rarefaction (Figures 5-6). Figure 6 demonstrates the utility of the phase-field formulation in converging to a sharp-interface solution. Namely, at intermediate (non-converged) SQP iterations, there are many regions of the domain where the materials are mixed (e.g., the phase variable takes values in $[0, 1]$), but at convergence, a sharp interface is obtained as the phase variable is either 0 or 1 (separated by the contact discontinuity). This also justifies the simplified mixture model in (39). Slices of the primitive variables at the final time $t = 0.1$ (Figure 7) show all variables are well-resolved with only minimal spurious oscillations, and both the shock and contact are represented as perfect discontinuities (except pressure and velocity, which are both constant across the contact). Figure 7 further confirms a sharp interface is obtained because the phase variable is 1 to the left of the contact discontinuity and 0 to the right of the discontinuity.

5.3. Ideal-stiffened gas Riemann problem

Next, we apply our method to a Riemann problem of (2) and (27) involving two different gases: an ideal gas with $\gamma_1 = 5/3$ and a stiffened gas with $\gamma_2 = 4.4$ and $P^* = 6 \times 10^8$. We consider the space-time domain $\Omega_x := (0, 1)$ and $\mathcal{T} = (0, 5 \times 10^{-5}]$ with initial condition

$$\rho(x, 0) = \begin{cases} 1200 & x < 0.5 \\ 1000 & x \geq 0.5 \end{cases}, \quad v(x, 0) = 0, \quad P(x, 0) = \begin{cases} 1 \times 10^9 & x < 0.5 \\ 1 \times 10^5 & x \geq 0.5 \end{cases}, \quad \phi(x, 0) = \begin{cases} 1 & x < 0.5 \\ 0 & x \geq 0.5 \end{cases}, \quad (75)$$

where standard international (SI) units are used for all variables. Because of the large pressure differential in the left and right states, there are fast moving waves that emanate from the initial discontinuity which cause a large disparity in the spatial and temporal scales. Therefore, we nondimensionalize the problem using the scalings $L^* = 1$, $t^* = 5 \times 10^{-4}$, and $m^* = 10^3$ (SI units).

A single slab is used to cover the entire time domain with an initial (non-aligned) space-time mesh consisting of 22 linear ($q = 1$) quadrilateral elements with quadratic ($p = 2$) solution approximation over each. The HOIST solver is initialized from the $p = 0$ DG solution on the initial space-time mesh. Similar behavior is observed for the ideal gas problem in Section 5.2, i.e., as the SQP iterations proceed, the faces of the mesh are driven towards alignment with the lead shock, contact discontinuity, and head and tail of the rarefaction (Figures 8-9). Figure 9 shows the phase-field formulation converges to a sharp-interface solution despite intermediate iterations containing non-trivial mixtures of the fluids. The grid is refined twice, each time by splitting each quadrilateral into four smaller ones (Figure 10); the space-time density

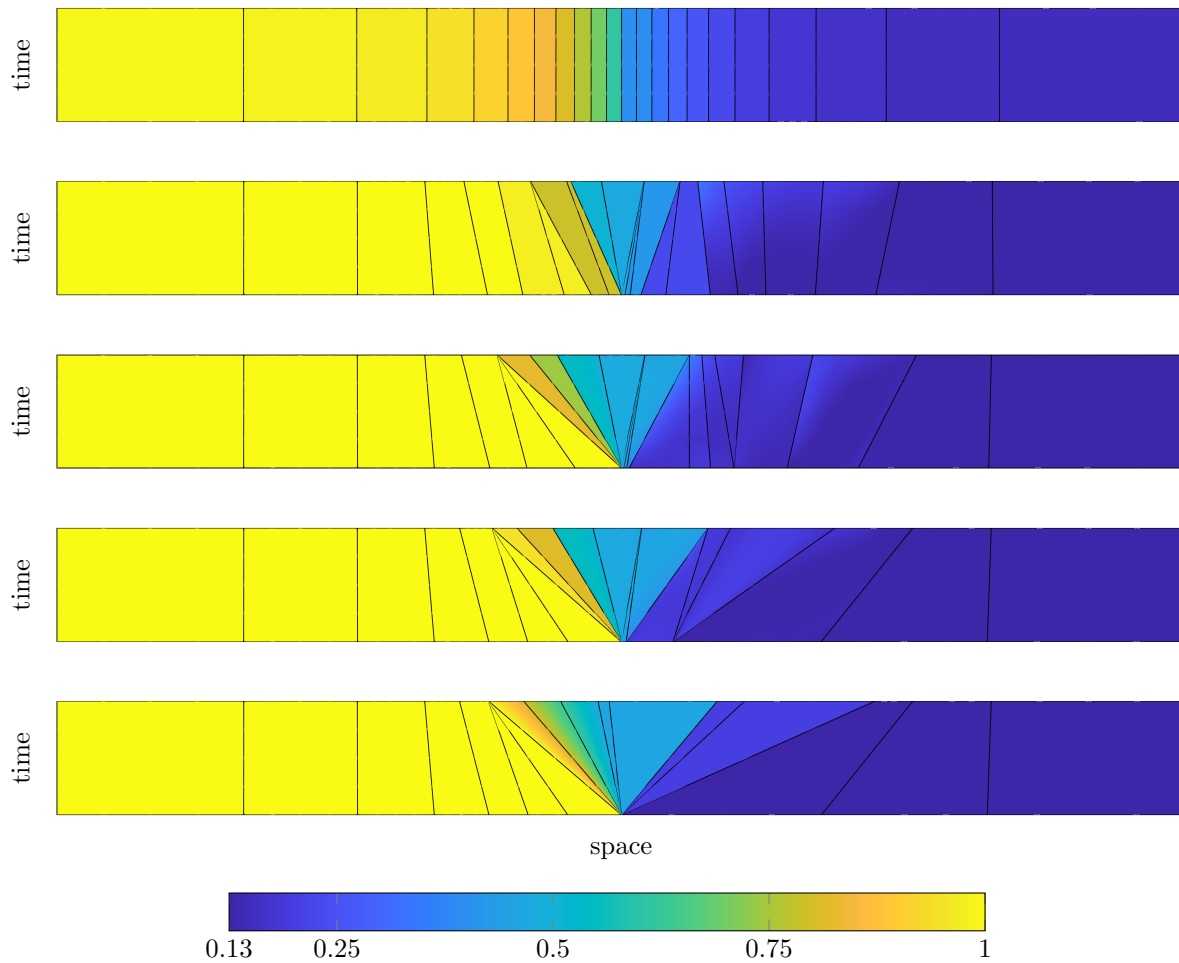


Figure 5: Two-phase HOIST SQP iterations (density) for two-phase, ideal gas Sod shock tube problem using one slab. SQP iterations $n = 0, 25, 50, 75, 100$ (*top-to-bottom*).

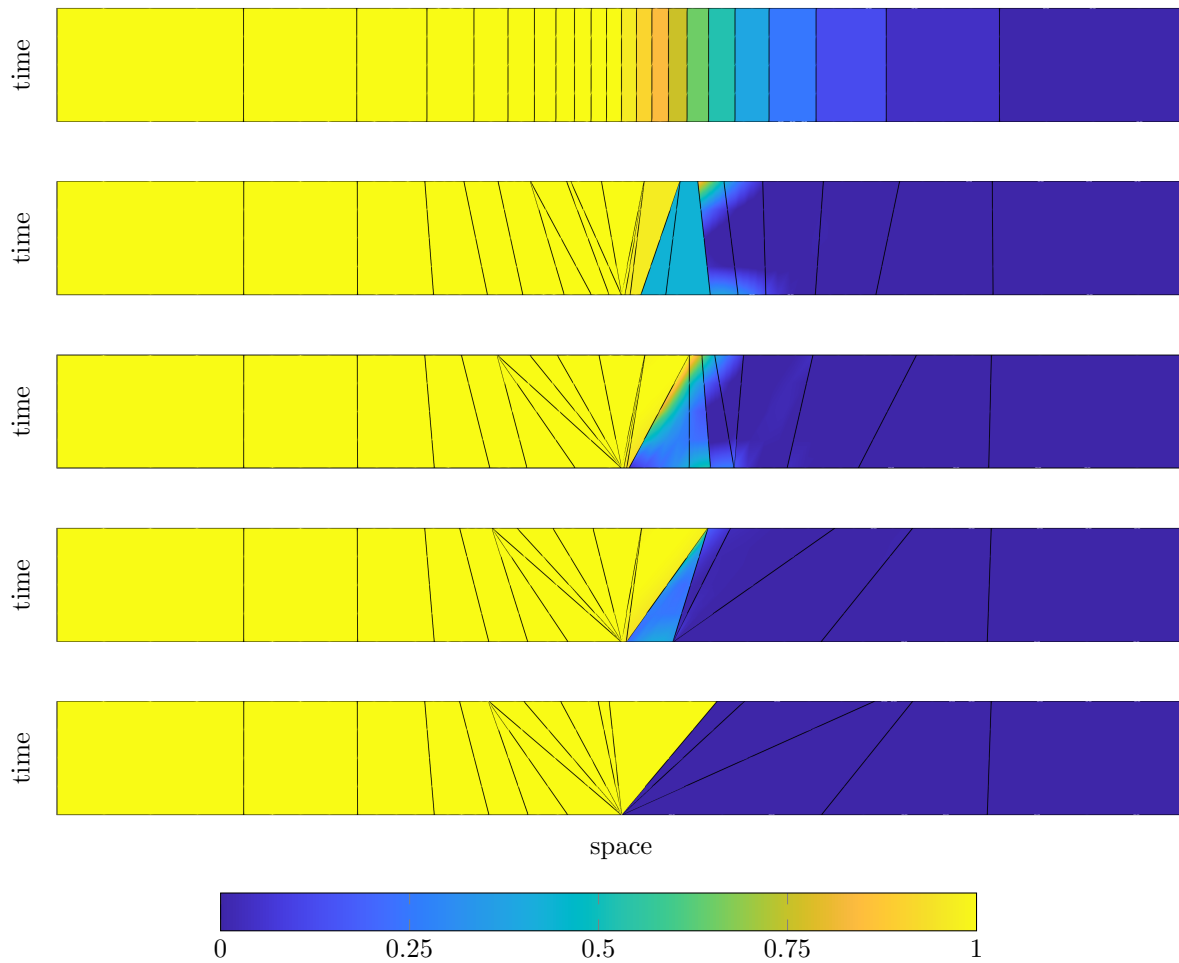


Figure 6: Two-phase HOIST SQP iterations (phase) for two-phase, ideal gas Sod shock tube problem using one slab. SQP iterations $n = 0, 25, 50, 75, 100$ (*top-to-bottom*).

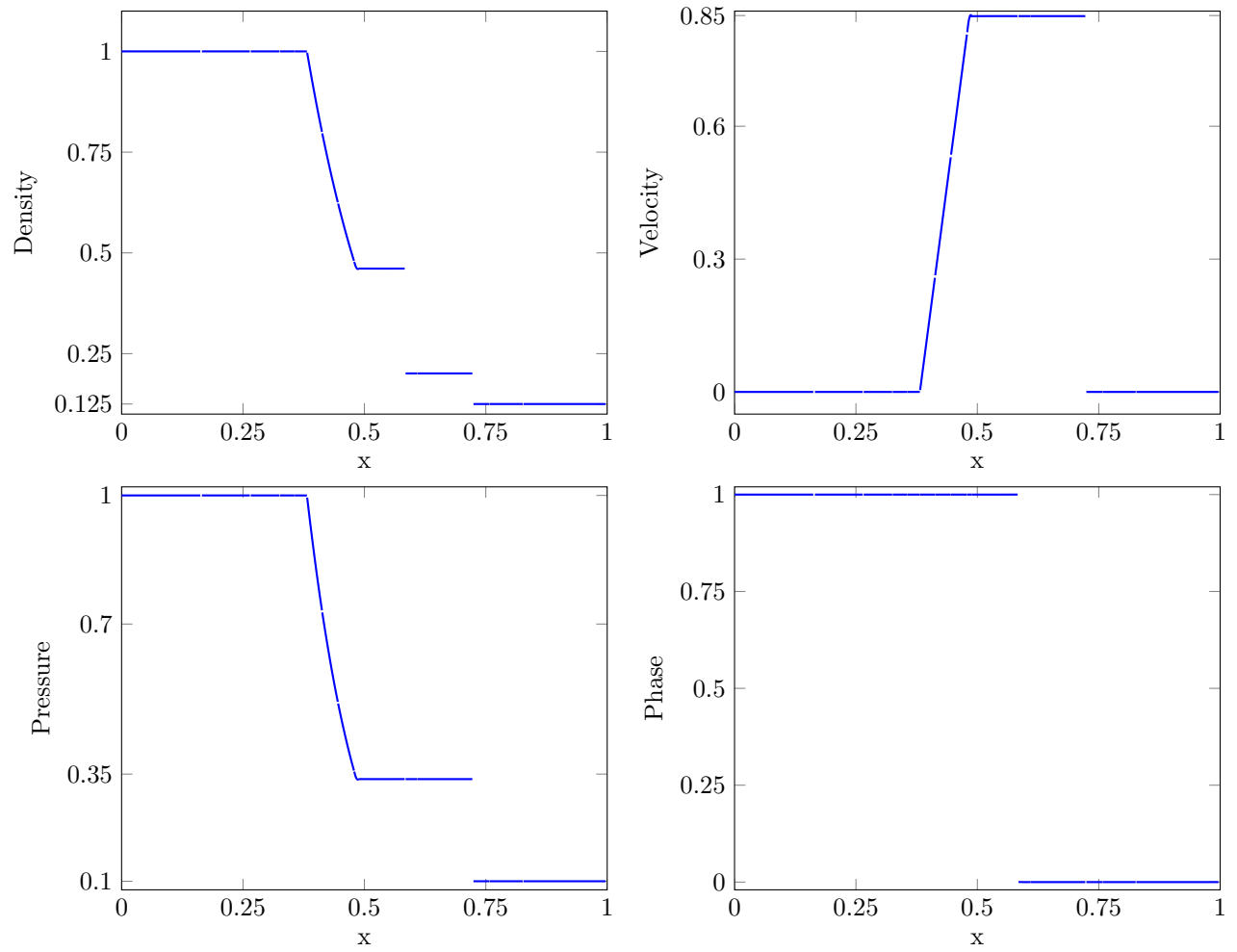


Figure 7: Slice of two-phase HOIST solution to the two-phase, ideal gas Sod shock tube problem at the final time.

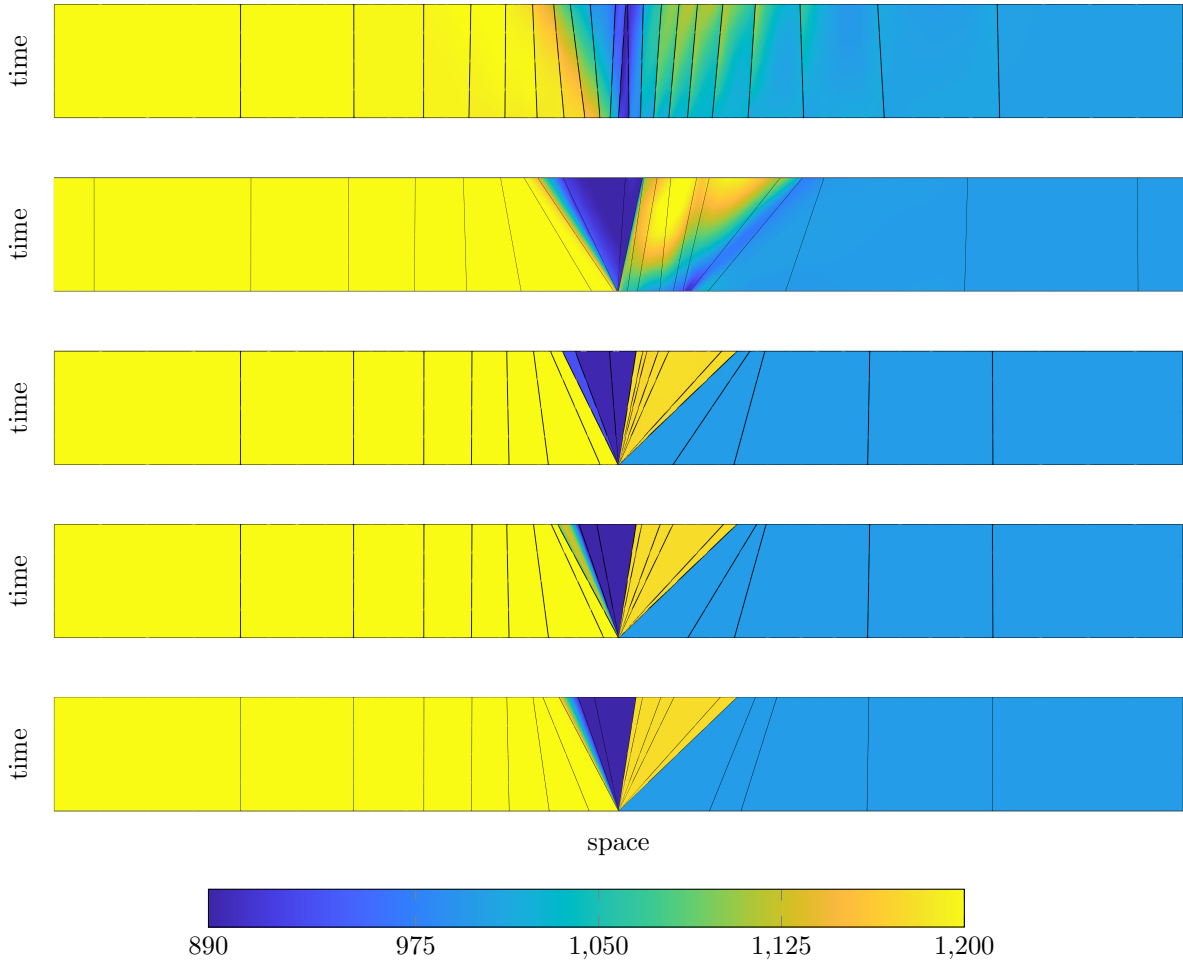


Figure 8: Two-phase HOIST SQP iterations (density) for ideal-stiffened gas Riemann problem using one slab. SQP iterations $n = 0, 10, 20, 30, 100$ (top-to-bottom).

compares well between the coarse (Figure 8) and intermediate/fine (Figure 10) grids. Slices of the primitive variables at the final time $t = 5 \times 10^{-5}$ (Figure 11) show all variables are well resolved with only minimal spurious oscillations, both the shock and contact are represented as perfect discontinuities (except pressure and velocity, which are both constant across the contact), and a sharp interface is obtain ($\phi(x, t) \in \{0, 1\}$). There is a minor rarefaction shock at the head of the rarefaction wave on the coarsest grid, most likely due to the large variation of density at the head and tail of the rarefaction and the single element approximation of the rarefaction at the final SQP iteration (Figure 8); however, this disappears under mesh refinement (Figure 11).

5.4. Spherically symmetric underwater explosion

Lastly, we consider a spherically symmetric underwater blast consisting of a high-pressure gas N_2 modeled using the BKW equation of state ($a = 0.0072051$ (J/mol/K²), $b = 23.4866$ (J/mol/K), $c = -9545$ (J/mol), $\beta = 0.403$, $\kappa = 10.86 \times 10^{-6}$ (m³ K ^{α} /mol), $\theta = 5441$ (K), $\alpha = 0.5$) and the surrounding water modeled as a stiffened gas ($\gamma_2 = 4.4$, $P_2^* = 6 \times 10^8$). The governing equations are the spherically symmetric two-phase

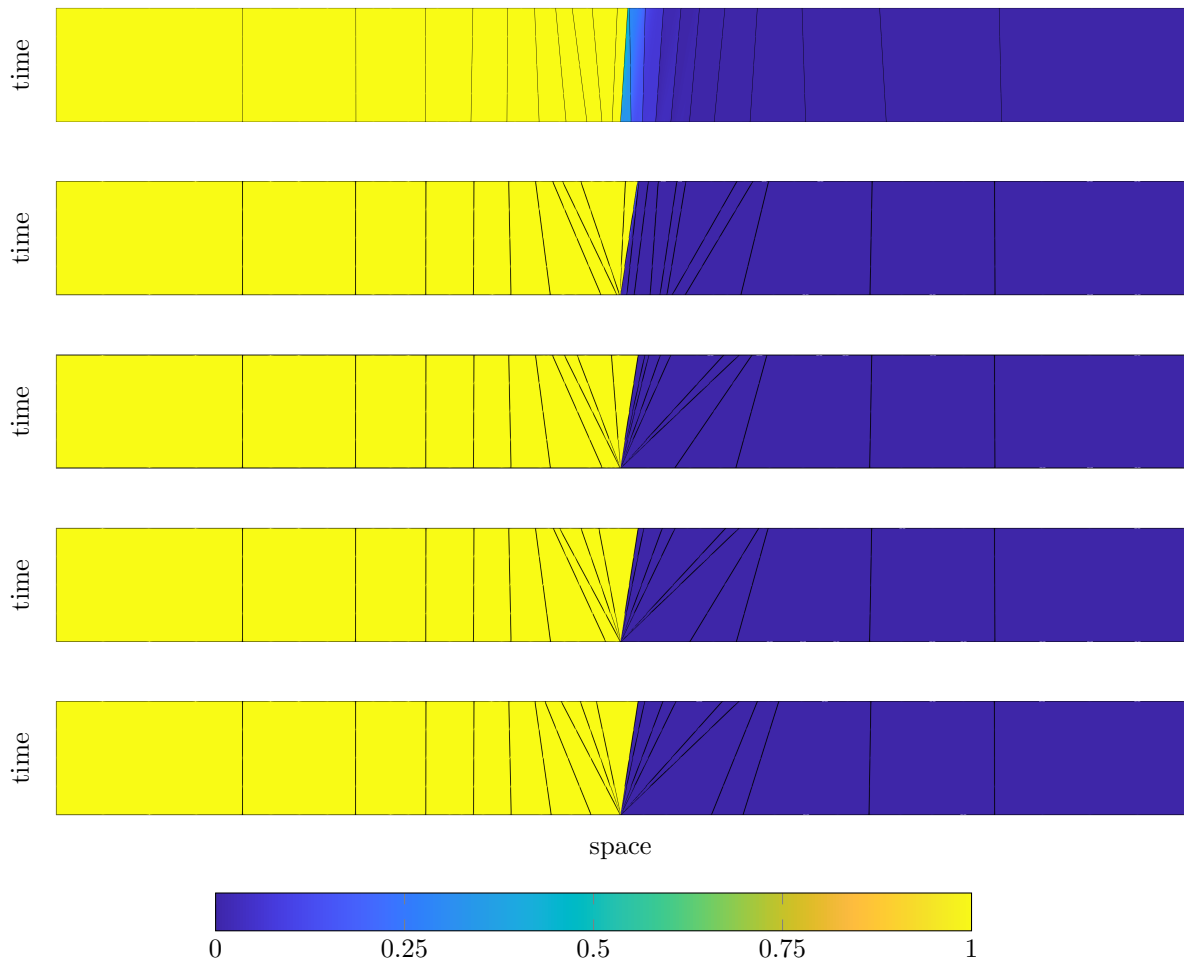


Figure 9: Two-phase HOIST SQP iterations (phase) for ideal-stiffened gas Riemann problem using one slab. SQP iterations $n = 0, 10, 20, 30, 100$ (*top-to-bottom*).

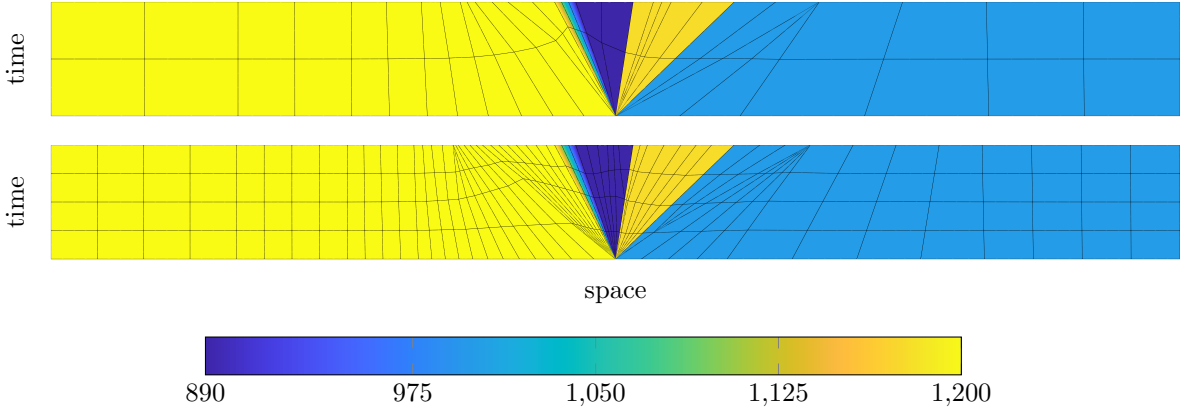


Figure 10: Two-phase HOIST solution (density) for ideal-stiffened gas Riemann problem using one slab after one (*top*) and two (*bottom*) levels of refinement relative to the original simulation in (8).

Euler equations, which are a time-dependent conservation law of the form (2) with

$$U_x = \begin{bmatrix} \rho \\ \rho v \\ \rho E \\ \rho \phi \end{bmatrix}, \quad \mathcal{F}_x(U_x) = \begin{bmatrix} \rho v \\ \rho v^2 + P(\rho, e) \\ [\rho E + P(\rho, e)] v \\ \rho \phi v \end{bmatrix}, \quad S_x(U_x) = -\frac{2}{r} \begin{bmatrix} \rho v \\ \rho v^2 \\ [\rho E + P(\rho, e)] v \\ \rho \phi v \end{bmatrix}, \quad (76)$$

where $\rho : \Omega_x \times \mathcal{T} \rightarrow \mathbb{R}_{\geq 0}$ is the density of the fluid, $v : \Omega_x \times \mathcal{T} \rightarrow \mathbb{R}$ is the radial velocity of the fluid, $E : \Omega_x \times \mathcal{T} \rightarrow \mathbb{R}$ is the total energy of the fluid, and $e : \Omega_x \times \mathcal{T} \rightarrow \mathbb{R}_{\geq 0}$ is the specific internal energy of the fluid. The pressure is defined by the mixture equation of state (39) with fluid 1 modeled as a BKW gas (Section 2.7.3) and fluid 2 modeled as water (Section 2.7.2). We consider the space-time domain $\Omega_x := (0, 1)$ and $\mathcal{T} = (0, 8 \times 10^{-4}]$ with initial condition

$$\rho(x, 0) = \begin{cases} 1600 & x < 0.5 \\ 1000 & x \geq 0.5 \end{cases}, \quad v(x, 0) = 0, \quad P(x, 0) = \begin{cases} 1.14 \times 10^{10} & x < 0.5 \\ 1 \times 10^5 & x \geq 0.5 \end{cases}, \quad \phi(x, 0) = \begin{cases} 1 & x < 0.5 \\ 0 & x \geq 0.5 \end{cases}, \quad (77)$$

where standard international (SI) units are used for all variables and, from these initial conditions, the temperature in the high-pressure region is 3000° . Because of the large pressure differential in the left and right states, there are fast moving waves that emanate from the initial discontinuity which cause a large disparity in the spatial and temporal scales. Therefore, we nondimensionalize the problem using the scalings $L^* = 1$, $t^* = 10^{-4}$, and $m^* = 10^2$.

Forty slabs are used to cover the time domain. The initial slab consists of 20 quadratic ($q = 2$) quadrilateral elements with quadratic ($p = 2$) solution approximation over each. Subsequent slabs may have a different number of elements due to element collapses [22, 40] during the HOIST iterations of the current slab and the extract-extrude-split approach introduced in [40] (Section 4); however, each slab has four layers of elements in the temporal dimension. A lead shock, rarefaction wave, and material interface separate the BKW gas from the water emanate from $x = 0.5$ (origin of the blast). The shock and material interface quickly travel away from the blast origin due to the large pressure differential and at some time $t > 0$, a secondary shock forms in the BKW phase. The secondary shock eventually over expands and reverses direction. The material interface decelerates as time evolves. The HOIST method produces a mesh in each space-time slab that aligns with the lead shock, rarefaction wave, material interface, and secondary shock (after its formation) (Figure 12). The motion of these features are tracked in time, including the dramatic motion of the secondary shock that changes direction and approaches the origin at the end of the time interval. The phase field clearly shows each slab converges to a sharp interface (Figure 13).

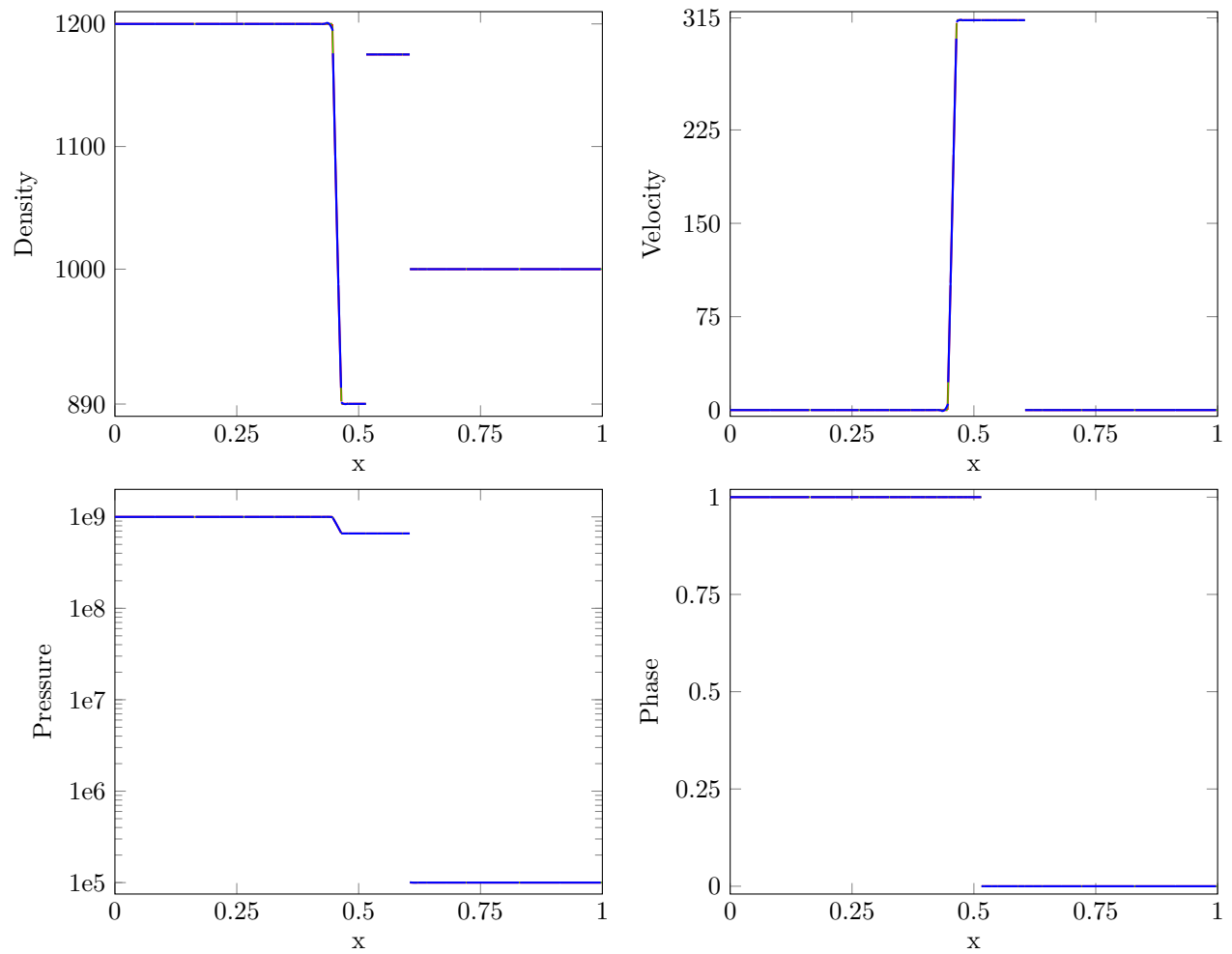


Figure 11: Slices of two-phase HOIST solution to the ideal-stiffened gas Riemann problem at the final time from the coarse (—), intermediate (—), and fine (—) meshes.

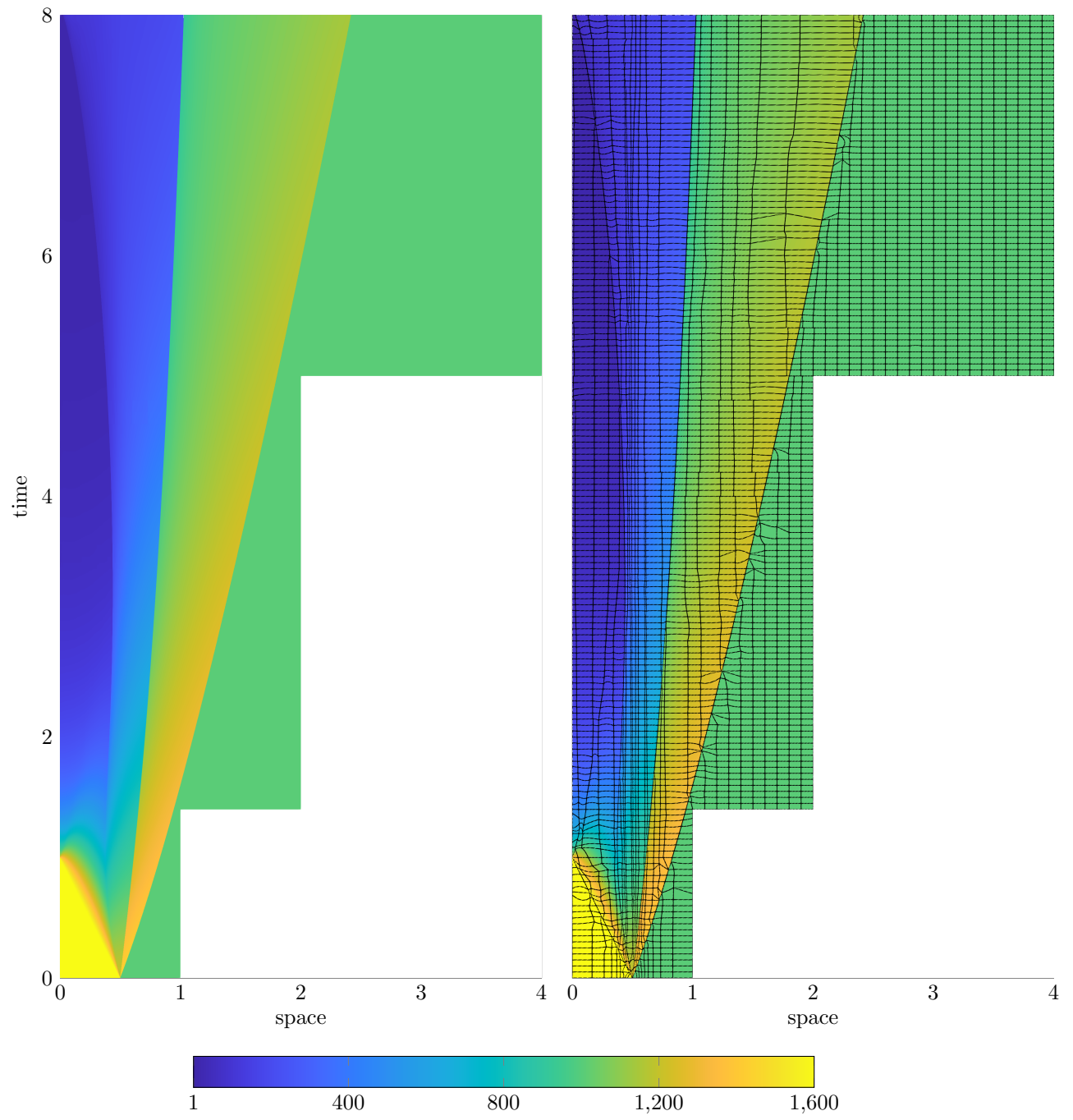


Figure 12: Two-phase HOIST solution (density) of the underwater blast problem, without (*left*) and with (*right*) edges shown.

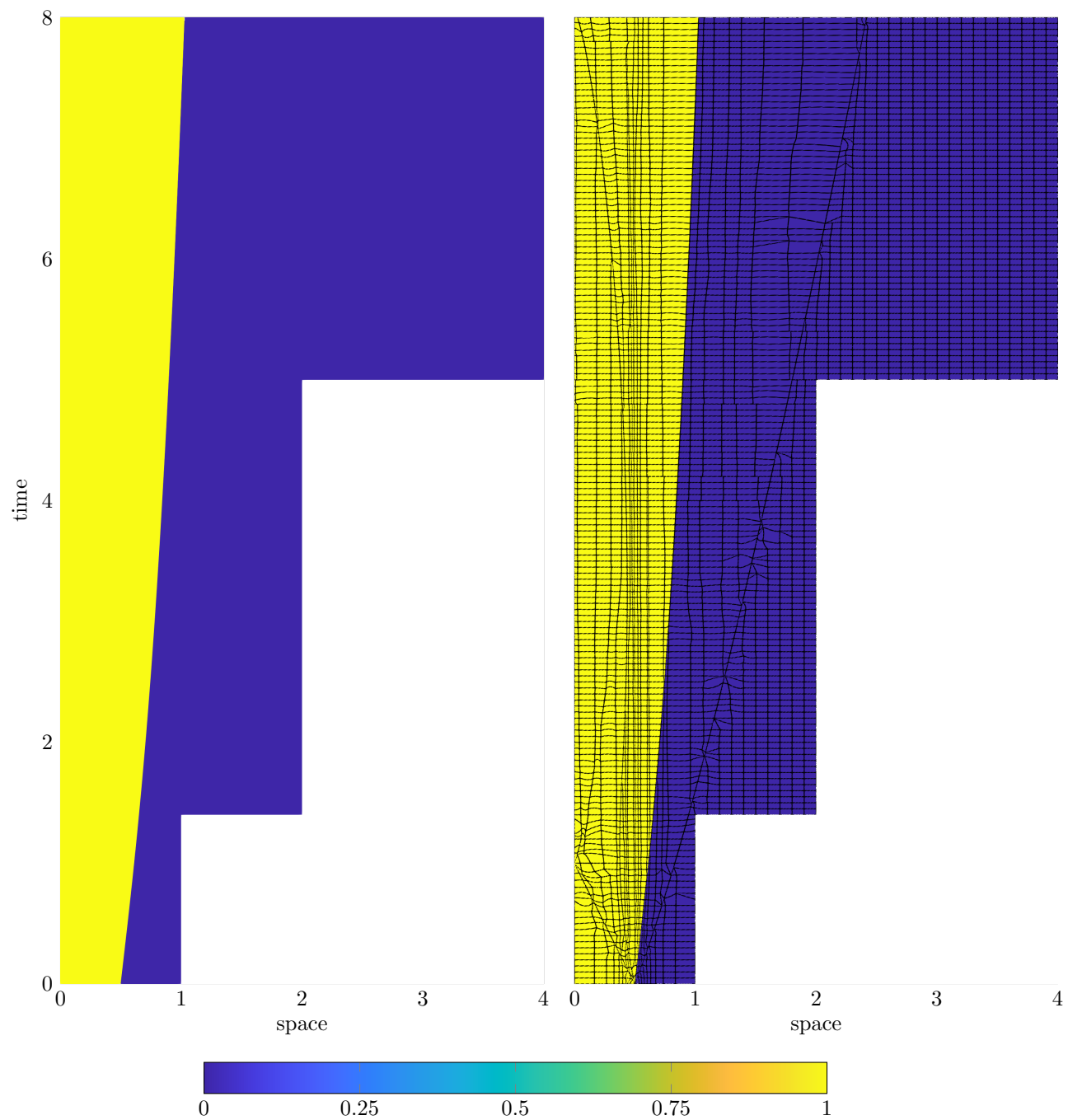


Figure 13: Two-phase HOIST solution (phase) of the underwater blast problem, without (*left*) and with (*right*) edges shown.

6. Conclusions

In this work, we develop a space-time implicit shock tracking method to simulate two-phase flow involving real gases. A unique feature of our method is it utilizes a phase-field formulation of the two-phase Euler equations to converge to a sharp-interface solution. That is, material mixtures $0 < \phi(x, t) < 1$ are only encountered at intermediate solver iterations; however, no mixtures $\phi(x, t) \in \{0, 1\}$ are present at the final iteration (solver convergence). As a result, the mixture equation of state must only recover the thermodynamic properties of the individual fluids in the limiting case where $\phi(x, t) \in \{0, 1\}$, which allows for an extremely simple mixture model (39). The proposed method is built on top of the space-time implicit shock tracking method in [40]. As such, it produces highly accurate, sharp-interface solutions to two-phase flows without artificial stabilization, even if the dynamics of shocks or material interface are complex.

The proposed method is validated using a single-phase and two-phase version of Sod's shock tube with ideal gases. Finally, the method is demonstrated on Riemann problems involving ideal and non-ideal (modeled with the Becker-Kistiakowsky-Wilson equation of state) gases and water (modeled as a stiffened gas). The space-time two-phase HOIST method successfully produces space-time slab meshes aligned with all shocks (even secondary shocks that form at time $t > 0$) and contacts, delivers highly accurate solutions on coarse meshes with all shocks and contacts represented as perfect discontinuities. For all problems considered, the phase field $\phi(x, t)$ converges to a sharp-interface solution where $\phi(x, t) \in \{0, 1\}$ for all $(x, t) \in \Omega_x \times \mathcal{T}$. Future research should investigate the proposed method for more complex two-phase flows in higher dimensions, such as the asymmetric collapse of underwater explosion bubbles, which is extremely challenging and computationally expensive to simulate using conventional methods.

Acknowledgments

This work is supported by AFOSR award numbers FA9550-20-1-0236, FA9550-22-1-0002, FA9550-22-1-0004, ONR award number N00014-22-1-2299, and NSF award number CBET-2338843. The content of this publication does not necessarily reflect the position or policy of any of these supporters, and no official endorsement should be inferred.

Appendix A. Ideal gas limit of real gas quantities

In this section we show the speed of sound and projected flux Jacobian in (20) for a real gas reduce to the well-known expressions [40] in the ideal gas limit. That is, we take the ideal gas equation of state (43) with partial derivatives (45). The derivatives of pressure under constant conservative variables are

$$\begin{aligned}\bar{P}_\rho(\rho, \rho v, \rho E) &= (\gamma - 1)(e - E + \|v\|^2) = (\gamma - 1) \|v\|^2 / 2 \\ \bar{P}_{\rho v}(\rho, \rho v, \rho E) &= -(\gamma - 1)v \\ \bar{P}_{\rho E}(\rho, \rho v, \rho E) &= (\gamma - 1).\end{aligned}\tag{A.1}$$

First, we substitute these expressions into the sound speed formula (24) to obtain

$$c^2 = (\gamma - 1) \left(H - \frac{1}{2} \|v\|^2 \right) = (\gamma - 1) \left(E + \frac{P}{\rho} - \frac{1}{2} \|v\|^2 \right) = (\gamma - 1) \left(e + \frac{P}{\rho} \right) = \gamma \frac{P}{\rho},\tag{A.2}$$

where the first equality results from direct substitution of the ideal gas equation of state into (24) and simplification, the next two equalities follow from the expressions for enthalpy and internal energy (16), and the final equality follows from the ideal gas equation of state (43) and simplification. This agrees with the speed of sound for an ideal gas.

Next, we substitute (A.1) into (20) to obtain

$$B_x(U_x, \eta_x) = \begin{bmatrix} 0 & \eta_x^T & 0 \\ -v_n v + \frac{(\gamma-1)}{2} \|v\|^2 \eta_x & v_n I_d + v \eta_x^T - (\gamma - 1) v \eta_x & (\gamma - 1) \eta_x \\ \frac{(\gamma-1)}{2} \|v\|^2 - H) v_n & H \eta_x^T - v_n (\gamma - 1) v^T & \gamma v_n \end{bmatrix},\tag{A.3}$$

which agrees with the projected inviscid flux Jacobian from [40]. Repeating this process with (22) yields

$$V_x(U_x, \eta_x) = \begin{bmatrix} 1 & \eta_x^T & 1 \\ v - c\eta_x & (v - \eta_x)\eta_x^T + I_d & v + c\eta_x \\ H - v_n c & v^T + (\theta - v_n)\eta_x^T & H + v_n c \end{bmatrix} \quad (\text{A.4})$$

with $\theta = \|v\|^2/2$, which agrees with the right eigenvectors of the projected inviscid flux Jacobian from [40]. Finally, repeating this process with (26) yields

$$V_x(U_x, \eta_x)^{-1} = \frac{\gamma - 1}{2c^2} \begin{bmatrix} \|v\|^2/2 + \frac{v_n c}{\gamma - 1} & -v^T - \frac{c}{\gamma - 1}\eta_x^T & 1 \\ \frac{2c^2}{\gamma - 1}(v_n \eta_x + \eta_x - v) - \|v\|^2 \eta_x & 2\eta_x v^T + \frac{2c^2}{\gamma - 1}(I_d - \eta_x \eta_x^T) & -2\eta_x \\ \|v\|^2/2 - \frac{v_n c}{\gamma - 1} & -v^T + \frac{c}{\gamma - 1}\eta_x^T & 1 \end{bmatrix}, \quad (\text{A.5})$$

where $H = \frac{c^2}{\gamma - 1} + \|v\|^2/2$ for an ideal gas was used to simplify the (2, 1) component. This expression agrees with the left eigenvectors of the projected inviscid flux Jacobian from [40]. The matrix of eigenvalues (25) is independent of P and agrees with the ideal gas eigenvalues in [40]. Thus, all terms in Section 2.4 reduce to the well-known expressions for an ideal gas when the ideal equation of state is used (43), which serves as a sanity check for the framework in this limiting case.

Appendix B. Speed of sound derivations

In this section we derive the speed of sound for a single-phase real gas (Appendix B.1) and a two-phase real gas using an arbitrary mixture equation of state (Appendix B.2). Furthermore, we prove the two-phase real gas sound speed reduces to the true material sound speeds in the limits $\phi \rightarrow 0$ and $\phi \rightarrow 1$ (Appendix B.3).

Appendix B.1. Speed of sound derivation, single-phase flow

For a single phase gas with arbitrary equation of state $P(\rho, e)$, the speed of sound, c , is defined as

$$c^2 = \left. \frac{\partial P}{\partial \rho} \right|_s, \quad (\text{B.1})$$

where s is the entropy. The Gibbs relation for the first law of thermodynamics states that the change in internal energy e of a system equals the heat added to the system less the work done by the system, i.e.,

$$Tds = de + Pdv, \quad (\text{B.2})$$

where $\nu = 1/\rho$ is the specific volume of the fluid. The change in the specific volume is related to the density change as $d\nu = -d\rho/\rho^2$, which reduces the Gibbs relation to

$$de = Tds + \frac{P}{\rho^2} d\rho. \quad (\text{B.3})$$

Because our equation of state is defined directly from density and internal energy, we have

$$dP = P_\rho d\rho + P_e de = P_\rho d\rho + P_e \left(Tds + \frac{P}{\rho^2} d\rho \right), \quad (\text{B.4})$$

where the Gibbs relation was used to eliminate de . Then, the pressure differential at constant entropy ($ds = 0$) is

$$dP \Big|_s = \left(P_\rho + P_e \left(\frac{P}{\rho^2} \right) \right) d\rho, \quad (\text{B.5})$$

which gives the following expression for the derivative of pressure with respect to density at constant entropy

$$\left. \frac{\partial P}{\partial \rho} \right|_s = P_\rho + P_e \left(\frac{P}{\rho^2} \right). \quad (\text{B.6})$$

Thus, the sound speed for a real gas with equation of state, $P(\rho, e)$, is

$$c = \sqrt{P_\rho + P_e \left(\frac{P}{\rho^2} \right)}. \quad (\text{B.7})$$

From the definition of enthalpy, we have $P/\rho^2 = (H - E)/\rho$, which reduces (B.7) to

$$c = \sqrt{P_\rho - \frac{P_e}{\rho} E + \frac{P_e}{\rho} H} = \sqrt{P_\rho - \frac{P_e}{\rho} (E - \|v\|^2) + \frac{P_e}{\rho} (H - \|v\|^2)} \quad (\text{B.8})$$

where the first equality comes directly from the substitution and the second equality comes from adding and subtracting $\frac{P_e}{\rho} \|v\|^2$ inside the radical. Using the definition of \bar{P}_ρ in (19), the expression for the sound speed reduces to

$$c = \sqrt{\bar{P}_\rho + \frac{P_e}{\rho} (H - \|v\|^2)}. \quad (\text{B.9})$$

Appendix B.2. Speed of sound derivation, two-phase flow

Now, consider an arbitrary two-phase flow equation of state, $P(\rho, e, \rho\phi)$. The sound speed definition (B.1) and Gibbs relations (B.2)-(B.3) are given in the previous section. Because our equation of state is defined directly from density, internal energy, and phase variable, we have

$$dP = P_\rho d\rho + P_e de + P_{\rho\phi} d(\rho\phi) = P_\rho d\rho + P_e \left(T ds + \frac{P}{\rho^2} d\rho \right) + P_{\rho\phi} \phi d\rho, \quad (\text{B.10})$$

where the Gibbs relation was used to eliminate de and constant material mixture ($d\phi = 0$) is assumed to simplify $d(\rho\phi)$. Then, the pressure differential at constant entropy ($ds = 0$) is

$$dP \Big|_s = \left(P_\rho + P_e \left(\frac{P}{\rho^2} \right) + \phi P_{\rho\phi} \right) d\rho, \quad (\text{B.11})$$

which gives the following expression for the derivative of pressure with respect to density at constant entropy

$$\frac{\partial P}{\partial \rho} \Big|_s = P_\rho + P_e \left(\frac{P}{\rho^2} \right) + \phi P_{\rho\phi}. \quad (\text{B.12})$$

Thus, the sound speed for a two-phase real gas with equation of state, $P(\rho, e, \rho\phi)$, for constant mixtures ($d\phi = 0$) is

$$c = \sqrt{P_\rho + P_e \left(\frac{P}{\rho^2} \right) + \phi P_{\rho\phi}}. \quad (\text{B.13})$$

From the definition of enthalpy, we have $P/\rho^2 = (H - E)/\rho$, which reduces (B.13) to

$$c = \sqrt{P_\rho - \frac{P_e}{\rho} E + \frac{P_e}{\rho} H + \phi P_{\rho\phi}} = \sqrt{P_\rho - \frac{P_e}{\rho} (E - \|v\|^2) + \frac{P_e}{\rho} (H - \|v\|^2) + \phi P_{\rho\phi}} \quad (\text{B.14})$$

where the first equality comes directly from the substitution and the second equality comes from adding and subtracting $\frac{P_e}{\rho} \|v\|^2$ inside the radical. Using the definition of \bar{P}_ρ in (19), the expression for the sound speed reduces to

$$c = \sqrt{\bar{P}_\rho + \frac{P_e}{\rho} (H - \|v\|^2) + \phi P_{\rho\phi}}. \quad (\text{B.15})$$

Appendix B.3. Proof of two-phase sound speed approaching true material sound speeds

In this section we prove the two-phase sound speed in (B.15) approaches the true material sound speeds in (B.9) in the limiting cases $\phi = 0$ and $\phi = 1$ assuming the mixture equation of state in (39). In particular, we will show

$$c|_{\phi=1} = \sqrt{\bar{P}_{1,\rho} + \frac{P_{1,e}}{\rho}(H - \|v\|^2)}, \quad c|_{\phi=0} = \sqrt{\bar{P}_{2,\rho} + \frac{P_{2,e}}{\rho}(H - \|v\|^2)}, \quad (\text{B.16})$$

where c is given by (B.15). From (40), the limiting cases of P_ρ are

$$P_\rho|_{\phi=1} = P_{1,\rho} + \frac{P_2 - P_1}{\rho}, \quad P_\rho|_{\phi=0} = P_{2,\rho}. \quad (\text{B.17})$$

From (41), the limiting cases of P_e are

$$P_e|_{\phi=1} = P_{1,e}, \quad P_e|_{\phi=0} = P_{2,e}. \quad (\text{B.18})$$

From (42), $P_{\rho\phi}$ is independent of ϕ and takes the value

$$P_{\rho\phi}|_{\phi=1} = P_{\rho\phi}|_{\phi=0} = \frac{P_1 - P_2}{\rho}. \quad (\text{B.19})$$

Direct substitution of these expressions into (30) for \bar{P}_ρ , we have

$$\bar{P}_\rho|_{\phi=1} = P_{1,\rho} + \frac{P_2 - P_1}{\rho} - \frac{P_{1,e}}{\rho}(E - \|v\|^2), \quad \bar{P}_\rho|_{\phi=0} = P_{2,\rho} - \frac{P_{2,e}}{\rho}(E - \|v\|^2). \quad (\text{B.20})$$

Combining (B.19) and (B.20), the limiting cases of $\bar{P}_\rho + \phi P_{\rho\phi}$ are

$$\begin{aligned} (\bar{P}_\rho + \phi P_{\rho\phi})|_{\phi=1} &= P_{1,\rho} + \frac{P_2 - P_1}{\rho} - \frac{P_{1,e}}{\rho}(E - \|v\|^2) + \frac{P_1 - P_2}{\rho} = P_{1,\rho} - \frac{P_{1,e}}{\rho}(E - \|v\|^2) \\ (\bar{P}_\rho + \phi P_{\rho\phi})|_{\phi=0} &= P_{2,\rho} - \frac{P_{2,e}}{\rho}(E - \|v\|^2). \end{aligned} \quad (\text{B.21})$$

Finally, we obtain (B.16) by direct substitution of (B.18) and (B.21) into (B.15).

Appendix C. Roe averages

In this section we present the Roe averages for Roe's approximate Riemann solver [51] for the real gas, single- and two-phase Euler equations using the Roe-Pike method [52] derived in [15]. The Roe averages are constructed such that the numerical flux function is conservative. In the ideal gas case, the Roe averages are defined for the density ($\hat{\rho}$), velocity (\hat{v}), and enthalpy (\hat{H}) as

$$\hat{\rho} = \sqrt{\rho_L \rho_R}, \quad \hat{v} = \frac{\sqrt{\rho_L} v_L + \sqrt{\rho_R} v_R}{\sqrt{\rho_L} + \sqrt{\rho_R}}, \quad \hat{H} = \frac{\sqrt{\rho_L} H_L + \sqrt{\rho_R} H_R}{\sqrt{\rho_L} + \sqrt{\rho_R}}. \quad (\text{C.1})$$

In this case, the partial derivatives of $P(\rho, e)$ can easily be expressed in term of these variables and the corresponding Roe averages are obtained by applying those expressions to (C.1).

On the other hand, the partial derivatives of $P(\rho, e)$ cannot be written in terms of the variables ρ , v , and H , which requires Roe averages for these partial derivatives to ensure the Roe flux is conservative. The Roe averages for the density, velocity, and enthalpy are given in (C.1) and the Roe averages for the partial derivatives are [15]

$$\begin{aligned} \hat{P}_\rho &= \begin{cases} \frac{1}{2\Delta\rho}(P_{RR} + P_{RL} - P_{LR} - P_{LL}) & \text{if } \Delta\rho \neq 0 \\ \frac{1}{2}(P_\rho(\rho, e_L) + P_\rho(\rho, e_R)) & \text{otherwise} \end{cases} \\ \hat{P}_e &= \begin{cases} \frac{1}{2\Delta e}(P_{RR} + P_{LR} - P_{RL} - P_{LL}) & \text{if } \Delta e \neq 0 \\ \frac{1}{2}(P_e(\rho_L, e) + P_e(\rho_R, e)) & \text{otherwise} \end{cases} \end{aligned} \quad (\text{C.2})$$

where $\Delta(\cdot) = \cdot_L - \cdot_R$ and $P_{ab} = P(\rho_a, e_b)$ for $a, b \in \{L, R\}$, $\rho = \rho_L = \rho_R$ in the case $\Delta\rho = 0$, and $e = e_L = e_R$ in the case $\Delta e = 0$. In finite precision, the check for $\Delta(\cdot) = 0$ is replaced with

$$\frac{\Delta(\cdot)}{\sqrt{(\cdot)_L^2 + (\cdot)_R^2}} \leq \tau, \quad (\text{C.3})$$

where τ is a relative tolerance ($\tau = 10^{-4}$ in this work). This is particularly important in this work where the left and right states can vary by nine orders of magnitude.

Finally, the Roe averages for the two-phase, real-gas Euler equations follows directly from the single-phase expressions. The Roe averages for density, velocity, and enthalpy agree with the ideal gas case (C.1) and the Roe average for the phase (ϕ) is defined consistently

$$\hat{\phi} = \frac{\sqrt{\rho_L}\phi_L + \sqrt{\rho_R}\phi_R}{\sqrt{\rho_L} + \sqrt{\rho_R}}. \quad (\text{C.4})$$

The Roe averages for the partial derivatives of pressure $P(\rho, e, \rho\phi)$ are

$$\begin{aligned} \hat{P}_\rho &= \begin{cases} \frac{1}{4\Delta\rho}(P_{RRR} + P_{RLL} + P_{RLR} + P_{RRL} - P_{LRR} - P_{LRL} - P_{LLR} - P_{LLL}) & \text{if } \Delta\rho \neq 0 \\ \frac{1}{4}(P_\rho(\rho, e_R, \rho\phi_R) + P_\rho(\rho, e_L, \rho\phi_R) + P_\rho(\rho, e_R, \rho\phi_L) + P_\rho(\rho, e_L, \rho\phi_L)) & \text{otherwise} \end{cases} \\ \hat{P}_e &= \begin{cases} \frac{1}{4\Delta e}(P_{RRR} + P_{LRR} + P_{RRL} + P_{LRL} - P_{RRL} - P_{LLR} - P_{RLL} - P_{LLL}) & \text{if } \Delta e \neq 0 \\ \frac{1}{4}(P_e(\rho_R, e, \rho\phi_R) + P_e(\rho_L, e, \rho\phi_R) + P_e(\rho_R, e, \rho\phi_L) + P_e(\rho_L, e, \rho\phi_L)) & \text{otherwise} \end{cases} \\ \hat{P}_{\rho\phi} &= \begin{cases} \frac{1}{2\Delta\rho\phi}(P_{RRR} + P_{LLR} - P_{RRL} - P_{LLL}) & \text{if } \Delta\rho\phi \neq 0 \\ \frac{1}{4}(P_{\rho\phi}(\rho_R, e_R, \rho\phi) + P_{\rho\phi}(\rho_R, e_L, \rho\phi) + P_{\rho\phi}(\rho_L, e_R, \rho\phi) + P_{\rho\phi}(\rho_L, e_L, \rho\phi)) & \text{otherwise,} \end{cases} \end{aligned} \quad (\text{C.5})$$

where $\Delta(\cdot) = \cdot_L - \cdot_R$ and $P_{abc} = P(\rho_a, e_b, \rho\phi_c)$ for $a, b, c \in \{L, R\}$, $\rho = \rho_L = \rho_R$ in the case $\Delta\rho = 0$, $e = e_L = e_R$ in the case $\Delta e = 0$, and $\rho\phi = \rho\phi_L = \rho\phi_R$ in the case $\Delta\rho\phi = 0$. In practice, (C.3) is used to numerically check for zero jumps.

References

- [1] Rémi Abgrall. How to prevent pressure oscillations in multicomponent flow calculations: a quasi conservative approach. *Journal of Computational Physics*, 125(1):150–160, 1996.
- [2] Rémi Abgrall and Smadar Karni. Computations of compressible multifluids. *Journal of Computational Physics*, 169(2):594–623, 2001.
- [3] Grégoire Allaire, Sébastien Clerc, and Samuel Kokh. A five-equation model for the simulation of interfaces between compressible fluids. *Journal of Computational Physics*, 181(2):577–616, 2002.
- [4] G.J. Ball, B.P. Howell, T.G. Leighton, and M.J. Schofield. Shock-induced collapse of a cylindrical air cavity in water: a free-Lagrangian simulation. *Shock Waves*, 10(4):265–276, 2000.
- [5] Jeffrey W. Banks, Donald W. Schwendeman, Ashwana K. Kapila, and William D. Henshaw. A high-resolution Godunov method for compressible multi-material flow on overlapping grids. *Journal of Computational Physics*, 223(1):262–297, 2007.
- [6] Garrett E. Barter and David L. Darmofal. Shock capturing with PDE-based artificial viscosity for DGFEM: Part I. Formulation. *Journal of Computational Physics*, 229(5):1810–1827, March 2010.
- [7] Carlos E. Baumann and J. Tinsley Oden. A discontinuous hp finite element method for the Euler and Navier–Stokes equations. *International Journal for Numerical Methods in Fluids*, 31(1):79–95, 1999.

- [8] Robert Becker. Stosswelle und detonation. *Zeitschrift für Physik*, 8(1):321–362, 1922.
- [9] I.L. Chern, J. Glimm, O. McBryan, B. Plohr, and S. Yaniv. Front tracking for gas dynamics. *Journal of Computational Physics*, 62(1):83–110, 1986.
- [10] Andrew Corrigan, Andrew Kercher, and David Kessler. A moving discontinuous Galerkin finite element method for flows with interfaces. *International Journal for Numerical Methods in Fluids*, 89(9):362–406, 2019.
- [11] Andrew T. Corrigan, Andrew Kercher, and David A. Kessler. The Moving Discontinuous Galerkin Method with Interface Condition Enforcement for Unsteady Three-Dimensional Flows. In *AIAA Scitech 2019 Forum*, AIAA SciTech Forum. American Institute of Aeronautics and Astronautics, January 2019.
- [12] Marcela Cruchaga, Diego Celentano, and Tayfun Tezduyar. A moving Lagrangian interface technique for flow computations over fixed meshes. *Computer Methods in Applied Mechanics and Engineering*, 191(6-7):525–543, 2001.
- [13] Marc T. Henry de Frahan, Sreenivas Varadan, and Eric Johnsen. A new limiting procedure for discontinuous Galerkin methods applied to compressible multiphase flows with shocks and interfaces. *Journal of Computational Physics*, 280:489–509, 2015.
- [14] Jean Donea, S.H.J.P. Giuliani, and Jean-Pierre Halleux. An arbitrary Lagrangian-Eulerian finite element method for transient dynamic fluid-structure interactions. *Computer Methods in Applied Mechanics and Engineering*, 33(1-3):689–723, 1982.
- [15] Paul Glaister. An approximate linearised Riemann solver for the Euler equations for real gases. *Journal of Computational Physics*, 74(2):382–408, 1988.
- [16] Keith A. Gonthier and Joseph M. Powers. A high-resolution numerical method for a two-phase model of deflagration-to-detonation transition. *Journal of Computational Physics*, 163(2):376–433, 2000.
- [17] Denis Gueyffier, Jie Li, Ali Nadim, Ruben Scardovelli, and Stéphane Zaleski. Volume-of-fluid interface tracking with smoothed surface stress methods for three-dimensional flows. *Journal of Computational Physics*, 152(2):423–456, 1999.
- [18] Cong-Tu Ha, Warn-Gyu Park, and Chul-Min Jung. Numerical simulations of compressible flows using multi-fluid models. *International Journal of Multiphase Flow*, 74:5–18, 2015.
- [19] Francis H. Harlow, J. Eddie Welch, et al. Numerical calculation of time-dependent viscous incompressible flow of fluid with free surface. *Physics of Fluids*, 8(12):2182, 1965.
- [20] Ami Harten, Bjorn Engquist, Stanley Osher, and Sukumar R. Chakravarthy. Uniformly high order accurate essentially non-oscillatory schemes, III. In *Upwind and High-Resolution Schemes*, pages 218–290. Springer, 1987.
- [21] Jan S. Hesthaven and Tim Warburton. *Nodal Discontinuous Galerkin Methods: Algorithms, Analysis, and Applications*. Texts in Applied Mathematics. Springer Science & Business Media, New York, 2007.
- [22] Tianci Huang and Matthew J. Zahr. A robust, high-order implicit shock tracking method for simulation of complex, high-speed flows. *Journal of Computational Physics*, 454:110981, April 2022.
- [23] P. Jenny, B. Müller, and H. Thomann. Correction of conservative Euler solvers for gas mixtures. *Journal of Computational Physics*, 132(1):91–107, 1997.
- [24] Eric Johnsen and Tim Colonius. Implementation of WENO schemes in compressible multicomponent flow problems. *Journal of Computational Physics*, 219(2):715–732, 2006.
- [25] Kamran Kamran, Riccardo Rossi, E. Onate, and S.R. Idelsohn. A compressible Lagrangian framework for the simulation of the underwater implosion of large air bubbles. *Computer Methods in Applied Mechanics and Engineering*, 255:210–225, 2013.

- [26] Smadar Karni. Viscous shock profiles and primitive formulations. *SIAM Journal on Numerical Analysis*, 29(6):1592–1609, 1992.
- [27] Smadar Karni. Multicomponent flow calculations by a consistent primitive algorithm. *Journal of Computational Physics*, 112(1):31–43, 1994.
- [28] Smadar Karni, Eduard Kirr, Alexander Kurganov, and Guergana Petrova. Compressible two-phase flows by central and upwind schemes. *ESAIM: Mathematical Modelling and Numerical Analysis*, 38(3):477–493, 2004.
- [29] Soshi Kawai and Hiroshi Terashima. A high-resolution scheme for compressible multicomponent flows with shock waves. *International Journal for Numerical Methods in Fluids*, 66(10):1207–1225, 2011.
- [30] Irfan Khan, Mingjun Wang, Yapei Zhang, Wenxi Tian, Guanghui Su, and Suizheng Qiu. Two-phase bubbly flow simulation using CFD method: A review of models for interfacial forces. *Progress in Nuclear Energy*, 125:103360, 2020.
- [31] G.B. Kistiakowsky and E. Bright Wilson. *The hydrodynamic theory of detonation and shock waves*. Office of the Publication Board, Department of Commerce, 1941.
- [32] Christiaan M. Klaij, Jaap J.W. van der Vegt, and Harmen van der Ven. Space-time discontinuous Galerkin method for the compressible Navier–Stokes equations. *Journal of Computational Physics*, 217(2):589–611, 2006.
- [33] Florian Kummer. Extended discontinuous Galerkin methods for two-phase flows: the spatial discretization. *International Journal for Numerical Methods in Engineering*, 109(2):259–289, 2017.
- [34] M.B. Liu and G.R. Liu. Smoothed particle hydrodynamics (SPH): an overview and recent developments. *Archives of Computational Methods in Engineering*, 17:25–76, 2010.
- [35] Xu-Dong Liu, Stanley Osher, and Tony Chan. Weighted essentially non-oscillatory schemes. *Journal of Computational Physics*, 115(1):200–212, November 1994.
- [36] Robert B. Lowrie, Philip L. Roe, and Bram Van Leer. Space-time methods for hyperbolic conservation laws. In *Barriers and Challenges in Computational Fluid Dynamics*, pages 79–98. Springer, 1998.
- [37] Ming Ma, Jiakai Lu, and Gretar Tryggvason. Using statistical learning to close two-fluid multiphase flow equations for a simple bubbly system. *Physics of Fluids*, 27(9), 2015.
- [38] Charles L. Mader. *Detonation properties of condensed explosives computed using the Becker-Kistiakowsky-Wilson equation of state*, volume 2900. Los Alamos Scientific Laboratory of the University of California, 1963.
- [39] Sean McKee, Murilo F. Tomé, Valdemir G. Ferreira, José A. Cuminato, Antonio Castelo, F.S. Sousa, and Norberto Mangiavacchi. The MAC method. *Computers & Fluids*, 37(8):907–930, 2008.
- [40] Charles J. Naudet and Matthew J. Zahr. A space-time high-order implicit shock tracking method for shock-dominated unsteady flows. *Journal of Computational Physics*, 501:112792, 2024.
- [41] Loann Neron and Richard Saurel. Revisiting the Becker-Kistiakowsky-Wilson equation of state. *Journal of Computational Physics*, page 113165, 2024.
- [42] Van-Tu Nguyen and Warn-Gyu Park. A free surface flow solver for complex three-dimensional water impact problems based on the VOF method. *International Journal for Numerical Methods in Fluids*, 82(1):3–34, 2016.
- [43] D.J. Nicklin. Two-phase bubble flow. *Chemical engineering science*, 17(9):693–702, 1962.
- [44] R. Nourgaliev, A. Corrigan, A. Kercher, S. Wopschall, and P. Greene. Implicit shock fitting for multi-material shock dynamics using a high-order space-time discontinuous finite-element method. Technical report, Lawrence Livermore National Lab.(LLNL), Livermore, CA (United States), 2021.

- [45] Stanley Osher and James A. Sethian. Fronts propagating with curvature-dependent speed: Algorithms based on Hamilton-Jacobi formulations. *Journal of Computational Physics*, 79(1):12–49, 1988.
- [46] Per-Olof Persson and Jaime Peraire. Sub-cell shock capturing for discontinuous Galerkin methods. In *44th AIAA Aerospace Sciences Meeting and Exhibit*, page 112, 2006.
- [47] James Edward Pilliod Jr and Elbridge Gerry Puckett. Second-order accurate volume-of-fluid algorithms for tracking material interfaces. *Journal of Computational Physics*, 199(2):465–502, 2004.
- [48] Joseph M. Powers. Two-phase viscous modeling of compaction of granular materials. *Physics of Fluids*, 16(8):2975–2990, 2004.
- [49] Joseph M. Powers, D.S. Stewart, and H. Krier. Theory of two-phase detonation—part I: modeling. *Combustion and Flame*, 80(3-4):264–279, 1990.
- [50] James J. Quirk and Smadar Karni. On the dynamics of a shock–bubble interaction. *Journal of Fluid Mechanics*, 318:129–163, 1996.
- [51] Philip L. Roe. Approximate Riemann solvers, parameter vectors, and difference schemes. *Journal of Computational Physics*, 43(2):357–372, 1981.
- [52] Philip L. Roe and J. Pike. Efficient construction and utilisation of approximate Riemann solutions. In *Proc. of the sixth int’l. symposium on Computing methods in applied sciences and engineering*, VI, pages 499–518, 1985.
- [53] Murray Rudman. Volume-tracking methods for interfacial flow calculations. *International Journal for Numerical Methods in Fluids*, 24(7):671–691, 1997.
- [54] Murray Rudman. A volume-tracking method for incompressible multifluid flows with large density variations. *International Journal for Numerical Methods in Fluids*, 28(2):357–378, 1998.
- [55] Richard Saurel and Rémi Abgrall. A simple method for compressible multifluid flows. *SIAM Journal on Scientific Computing*, 21(3):1115–1145, 1999.
- [56] Richard Saurel, Fabien Petitpas, and Ray A. Berry. Simple and efficient relaxation methods for interfaces separating compressible fluids, cavitating flows and shocks in multiphase mixtures. *Journal of Computational Physics*, 228(5):1678–1712, 2009.
- [57] Robert I. Saye. Implicit mesh discontinuous Galerkin methods and interfacial gauge methods for high-order accurate interface dynamics, with applications to surface tension dynamics, rigid body fluid–structure interaction, and free surface flow: Part I. *Journal of Computational Physics*, 344:647–682, 2017.
- [58] Robert I. Saye and James A. Sethian. Multiscale modeling of membrane rearrangement, drainage, and rupture in evolving foams. *Science*, 340(6133):720–724, 2013.
- [59] Andrew Shi, Per-Olof Persson, and Matthew J. Zahr. Implicit shock tracking for unsteady flows by the method of lines. *Journal of Computational Physics*, 454:110906, 2022.
- [60] G. Shobeyri and M.H. Afshar. Simulating free surface problems using discrete least squares meshless method. *Computers & Fluids*, 39(3):461–470, 2010.
- [61] Keh-Ming Shyue. An efficient shock-capturing algorithm for compressible multicomponent problems. *Journal of Computational Physics*, 142(1):208–242, 1998.
- [62] Muhamed Suceca, Hay Yee Serene Chan, Barbara Stimac, and Mario Dobrilovic. BKW EOS: History of modifications and further improvement of accuracy with temperature-dependent covolumes of polar molecules. *Propellants, Explosives, Pyrotechnics*, 48(1):e202100278, 2023.

- [63] J.J. Sudirham, Jacobus J.W. van der Vegt, and Rudolf M.J. van Damme. Space–time discontinuous Galerkin method for advection–diffusion problems on time-dependent domains. *Applied Numerical Mathematics*, 56(12):1491–1518, 2006.
- [64] Ying Sun and Christoph Beckermann. Sharp interface tracking using the phase-field equation. *Journal of Computational Physics*, 220(2):626–653, 2007.
- [65] Zhe Sun, K. Djidjeli, Jing T. Xing, et al. Modified MPS method for the 2D fluid structure interaction problem with free surface. *Computers & Fluids*, 122:47–65, 2015.
- [66] Mark Sussman and Emad Fatemi. An efficient, interface-preserving level set redistancing algorithm and its application to interfacial incompressible fluid flow. *SIAM Journal on Scientific Computing*, 20(4):1165–1191, 1999.
- [67] Mark Sussman, Peter Smereka, and Stanley Osher. A level set approach for computing solutions to incompressible two-phase flow. *Journal of Computational Physics*, 114(1):146–159, 1994.
- [68] S.P. Van der Pijl, A. Segal, C. Vuik, and P. Wesseling. A mass-conserving level-set method for modelling of multi-phase flows. *International Journal for Numerical Methods in Fluids*, 47(4):339–361, 2005.
- [69] Bram Van Leer. Towards the ultimate conservative difference scheme. V. A second-order sequel to Godunov’s method. *Journal of Computational Physics*, 32(1):101–136, 1979.
- [70] Cheng Wang, Xiangxiong Zhang, Chi-Wang Shu, and Jianguo Ning. Robust high order discontinuous Galerkin schemes for two-dimensional gaseous detonations. *Journal of Computational Physics*, 231(2):653–665, 2012.
- [71] Samuel W.J. Welch and John Wilson. A volume of fluid based method for fluid flows with phase change. *Journal of Computational Physics*, 160(2):662–682, 2000.
- [72] Jan H. Witte. Mixing shocks in two-phase flow. *Journal of Fluid Mechanics*, 36(4):639–655, 1969.
- [73] Matthew J. Zahr and Per-Olof Persson. An optimization-based approach for high-order accurate discretization of conservation laws with discontinuous solutions. *Journal of Computational Physics*, 365:105–134, July 2018.
- [74] Matthew J. Zahr, Andrew Shi, and Per-Olof Persson. Implicit shock tracking using an optimization-based high-order discontinuous Galerkin method. *Journal of Computational Physics*, 410:109385, 2020.